Fine ultrafiltration of concentrated oligosaccharide solutions – Hydration and pore size distribution effects

Aguirre Montesdeoca, V., Janssen, A. E. M., Boom, R. M., & van der Padt, A.

Fine ultrafiltration of concentrated oligosaccharide solutions – hydration and pore size distribution effects

Victor Aguirre Montesdeoca*[1,2], Anja E. M. Janssen[2], R. M. Boom[2] and A. Van der Padt[2,3]

[1]Institute for Sustainable Process Technology, P.O. Box 247, 3800 AE, Amersfoort, The Netherlands.

[2]Wageningen University, Food Process Engineering Group, P.O. Box 17, 6700 AA, Wageningen, The Netherlands.

[3] FrieslandCampina, P.O. Box 1551, 3800 BN, Amersfoort, The Netherlands.

*Corresponding Author: E-mail: victor.aguirremontesdeoca@wur.nl

ABSTRACT

The effects of high concentration in the fine ultrafiltration of a solution of oligosaccharides were investigated both experimentally and using a mass transfer model based on the Maxwell-Stefan equations. At high concentrations, negative retentions were found for the smaller sugars, which cannot be ascribed to effects of ionic interaction, membrane adsorption or fouling. Instead, the behaviour could be quantitatively described by incorporating the effects of the thermodynamic non-ideality of the solutions and the effects of the pore size distribution. Experiments were performed to validate the model using as feed an oligosaccharide mixture with a concentration up to a 35% w/w. The model predictions allows the identification of an optimum feed concentration at which the efficiency of the separation is maximized. The results show that the fine ultrafiltration of sugars can be well described and predicted when taking into account the relevant thermodynamic interactions, the membrane pore size distribution and pressure effects.

Keywords: High concentration; oligosaccharides; hydration; pore size distribution; Maxwell-Stefan equations.

1. INTRODUCTION

Ultrafiltration (UF) applications are not restricted to water treatment, UF is increasingly used in the food and biotechnology industry for purification and concentration of streams. Its main advantages are its simplicity, low costs and eco-efficiency [1]. In order to seize this potential, a complete understanding of the involved mechanisms is required, becoming essential a mathematical representation of the process for proper design, control and optimization.

Various models have been derived to describe NF and UF. They are often based on simplified considerations such as single solute mixtures and diluted conditions, with the Steric Pore Model and the Kedem-Katchalsky equations being the most common ones [2, 3]. Food streams, however, are complex non-ideal multicomponent solutions that frequently do not comply with the simplifications considered in the aforementioned models. Therefore, more rigorous considerations are needed for the development of a more realistic representation of the NF/UF of complex food streams.

The combination of the multicomponent nature of food streams and the high solute concentration determines physicochemical interactions that make the system thermodynamically non-ideal [4]. In general, these interactions can be classified into three types: Interactions with the membrane, interactions between different solute molecules and interactions between solutes and solvent molecules. Many studies about the interactions with the membrane can be found in literature especially for separation of ionic solutions. The membrane charge is here normally used as a fitting parameter that depends on the nature and concentration of the solutes inside the membrane [2, 5, 6]. The other two types of interactions have received less attention and are often neglected by authors even when modelling systems at high concentrations [7, 8].

Only few filtration studies can be found in literature in which the effect of different solutes on each other is assessed. Van Oers et al. (1997) described the decrease in the observed PEG rejection when combined with dextran in comparison with the observed rejection of PEG as single solute [9]. During these experiments, these authors even obtained negative observed rejection values for PEG under some specific conditions. Likewise, Bargeman et al. (2005) and Luo (2011) showed a decrease in the observed rejection of glucose when NaCl was added in the feed mixture [6, 10]. This influence of the

solutes on each other rejection is not necessarily due to a direct interaction between solutes, but may also be caused by interactions between solutes and solvent, which in case of aqueous streams, can be ascribed to hydration [11, 12]. The hydration phenomena has a direct influence on the effective size of the solute molecules and on the amount of free water in the system [11, 12]. In a recent study, we assessed the impact of hydration on the size of sugar molecules and on their permeation at diluted conditions [13]. At high concentrations, the effects of hydration on the system thermodynamics are expected to be larger [4].

We here therefore assess the effect of high concentrations on the performance of multicomponent fine UF systems. We develop a mathematical model based on the Maxwell Stefan Equations to account for the diffusive coupling effects between solutes in the concentration polarization layer. Experimental data is obtained using a fructooligosaccharides mixture with a range of polymerization degrees from1 to 7 as feed, from which we aim to remove the mono- and disaccharides. All components of the mixture and the membrane are neutral, thus electrical interactions are ruled out of this study.

2. THEORETICAL ASPECTS

In order to model a concentrated UF system we can be envisage it as two phases: the liquid phase and the membrane. The liquid phase includes the concentration polarization layer just in front of the membrane, in which the concentration of solutes is the highest and the system is thermodynamically non-ideal. Inside the membrane, the solute concentration is lower, and mass transfer may be assumed to take place through non-uniform cylindrical pores [2]. The concentration polarization layer and the membrane can be considered to be at thermodynamic equilibrium at the membrane interface.

2.1 Transport in the concentration polarization layer

Concentration polarization in diluted systems can be represented by the film model (Eq.1), which is derived from a solute mass balance over the thickness of the concentration polarization layer.

$$\frac{C_w - C_p}{C_b - C_p} = \exp\left(\frac{J}{k}\right), \quad (1)$$

in which J is the total flux trough the membrane (mostly water), k is the mass transfer coefficient and C_w , C_b and C_p are the concentrations at the membrane surface, in the bulk of the retentate and in the permeate, respectively.

When the system is concentrated, however, the film model cannot be used since it considers the solute fluxes to be independent of each other. In concentrated systems, diffusional coupling takes place and the transport of one solute is influenced by that of other solutes. Consequently, the so-called Maxwell-Stefan equations are much more suitable for concentrated multicomponent mixtures[14, 15]. These equations represent a force balance in which the driving force exerted on a species is counteracted by the friction with all the other species present in the system. In this approach cross effects between components are considered, and thermodynamic considerations that account for the non-ideality can also be incorporated into the equations. Taylor and Krishna made a complete description of the Maxwell Stefan equations and their application [16].

A convenient way to express the Maxwell Stefan equations is shown in Eq. 2, in which the force balance in the concentration polarization layer for molecule i is described. Thus, the molecular diffusion in this layer can be represented by a set of $m-1$ equations, m being the number of components (including water as component m). The left side of the equation represents the driving forces for solute i and the term at the right side represents the friction forces working over solute i. It is important to realize that the driving forces are expressed with the chemical potential gradient ($\nabla\mu_i$) and pressure gradient (∇P). x represents the solutes mole fraction, $\bar{v}$ the molar volumes of the hydrated molecules and u are their linear velocities. $Đ_{ij}$ is the Maxwell Stefan cross diffusion coefficient between species i and j [16].

$$x_i\left(\frac{1}{RT}\nabla_{T,P}\mu_i + \frac{\bar{v}_i}{RT}\nabla P\right) = -\sum_{\substack{j=1 \\ j\neq i}}^{m} \frac{x_i x_j (u_i - u_j)}{Đ_{ij}} \quad (2)$$

The chemical potential gradient has been worked out in Eq. 3 and it is shown that the mole fraction gradient of every solute has an effect on the driving force of molecule i. Additionally, the term containing the pressure gradient has been removed because the pressure can be considered approximately constant in the concentration polarization layer ($\nabla P = 0$). At the right side, the friction term has been adapted to molar fluxes (N), considering that $N_i = C_T x_i u_i$, in which C_T is the total molar concentration.

$$\sum_{j=1}^{m-1} \left(\delta_{ij} + x_i \frac{\partial \ln \gamma_i}{\partial x_j} \right)_{T,P} \frac{dx_j}{dz} = \sum_{\substack{j=1 \\ j \neq i}}^{m} \frac{(x_i N_j - x_j N_i)}{C_T \, Đ_{ij}} \tag{3}$$

The term inside brackets in the left side of Eq. 3 is known as the thermodynamic factor (Γ_{ij}), in which δ_{ij} is the Kronecker delta. Γ_{ij} is a function of the change in the solute activity coefficient γ_i and represents the interaction between species i and j. For ideal systems $\Gamma_{ij} = 0$ when $i \neq j$, meaning that no interaction takes place between species, and $\Gamma_{ij} = 1$ when $i = j$. Hence, in ideal systems, the driving force of molecule i is its own molar fraction gradient $\frac{dx_i}{dz}$ as shown in Eq. 4.

$$\sum_{j=1}^{m-1} \Gamma_{ij} \frac{dx_j}{dz} = \sum_{\substack{j=1 \\ j \neq i}}^{m} \frac{(x_i N_j - x_j N_i)}{C_T \, Đ_{ij}} \tag{4}$$

Kooijman and Taylor (1991) obtained a relation (Eq. 5) to estimate the Maxwell-Stefan cross diffusion coefficients ($Đ_{ij}$) based on easily measurable binary diffusion coefficients ($Đ_{im}$)[17]. The accuracy of this relation was found to be superior to other relations found in the literature; they were assessed in the work of Liu et al. using Equilibrium Molecular Dynamics simulations [18].

$$Đ_{ij}^{x_m \to 1} = \sqrt{Đ_{im}^{x_m \to 1} Đ_{jm}^{x_m \to 1}} \tag{5}$$

It is important to notice that even for aqueous concentrated systems, the molar fraction of component m (water) is still close to 1 due to the great difference in molecular weight between solutes and water.

Therefore, $Đ_{im}^{x_m \to 1}$ can be considered to be similar to the Fick diffusion coefficient under diluted conditions D_i^{∞}, which can be easily found in literature.

In order to numerically solve Eq. 4, a uniform concentration polarization layer thickness (δ) should be considered for all the diffusing components. δ can be calculated using the so-called Sherwood relations considering the viscosity of the retentate stream (Appendix A).

2.1.1 Thermodynamic non-idealities (Hydration).

To account for the non-idealities due to high concentration in the concentration polarization layer we consider the effect of hydration. It has been repeatedly described in literature that the non-idealities in concentrated sugar solutions up to 60° Brix can be explained by just considering the hydration effect on the solutes [11, 19, 20]. During hydration, sugars bind water molecules, 'removing' them from the solvent. As consequence of this reduction in the effective number of molecules, the activity coefficient of the solutes in the mixture increases. This is also known as "salting out effect", and is commonly used to precipitate proteins by adding salts to a protein solution [21].

The activity coefficients (γ_i) of a solute can be related to its hydration by using Eq. 6, which is derived in detail in Appendix B. Here, h_f represents the hydration number of each segment of the oligosaccharides, which is a parameter that can be easily found in literature. The value used for fructose (the common segment for all the solutes) was 3.8 [22, 23]. s_i represents the number of segments (monomers) in the oligosaccharide chain. The fraction x_{seg} is the number (moles) of segments in the solution divided by the overall number of moles.

$$\gamma = \frac{1}{1 - h_f \, x_{seg}} \tag{6}$$

$$x_{seg} = \sum_{i=1}^{m-1} x_i \, s_i$$

The obtained value for γ holds for all the solutes in the mixture because all of them are influenced by the hydration effect in the same manner. In other words, sugar species with different degree of polymerization bind different numbers of water molecules, but the total number of bound water molecules affects the thermodynamics of all the components to the same extent. By taking the derivative with respect to x_{seg}, the following expression can be obtained.

$$\frac{\partial \ln \gamma}{\partial x_{seg}} = \frac{h_f}{1 - h_f x_{seg}} \tag{7}$$

The equation above can be used to fit in the thermodynamic factor Γ_{ij} as it was defined in Eq. 3.

$$\Gamma_{ij} = \delta_{ij} + s_j \frac{\partial ln\gamma_i}{\partial x_{seg}} x_i \tag{8}$$

Although C_T is usually considered constant in the Maxwell Stefan equations, when the polarization is high, C_T may differ significantly over the thickness of the concentration polarization layer. Eq. 9 has been derived to estimate C_T using the local molar fractions. At the right hand side of the equation, the first term represents the volume occupied by all the hydrated sugars ($m-1$ components) for 1 mol of mixture. The second term is the volume of the 'non-removed' (free) water for 1 mol of mixture. $\bar{v}_i$ stands for the hydrated molar volume of the sugars and $\bar{v}_m$ is the molar volume of water.

$$\frac{1}{C_T} = \sum_{i=1}^{m-1} x_i \bar{v}_i + \left(1 - \sum_{i=1}^{m-1} x_i - \sum_{i=1}^{m-1} x_i \, s_i h_f\right) \bar{v}_m \tag{9}$$

2.2 Interface

The concentration inside the pores is lower than in the outside due to the existence of an excluded volume adjacent to the pore walls that is not accessible to the centre of the incoming molecules [24]. This defines a steric hindrance ($\hat{\phi}$), which is exclusively dependent on the geometries of the pore and

of the transient molecule. For spherical molecules and cylindrical pores, $\hat{\phi}$ can be derived using Eq. 10 [25, 26]. Here r_i is the radius of the transient molecule, which is normally represented by the Stokes radius when the molecule is spherical. In this case, since oligosaccharides molecules are elongated, an averaged radius r_G based on a capsular shape will be calculated; this approach is explained in detail in our previous study [13].

$$\hat{\phi}_i = \left(1 - \frac{r_i}{r_{pore}}\right)^2 \tag{10}$$

Only for neutral molecules and under diluted conditions, it can be stated that $\hat{\phi}_i$ is similar to the partition of the solute at the interface, φ_i. At concentrated conditions, other factors such as the thermodynamic non-idealities can have an effect on φ_i. To analyse this scenario is necessary to consider that under steady state conditions, local thermodynamic equilibrium can be assumed at the membrane interface. Hence, the chemical potential for each species is considered the same at the membrane surface (w) and just inside the pore ($'$) as represented in Eq. 11.

$$\mu_i^w = \mu_i' \tag{11}$$

$$RTlna_i^w + \bar{v}_i P = RTlna_i' + \bar{v}_i P'$$

$$a_i^w = a_i'$$

$$x_i^w \gamma_i^w = x_i' \gamma_i'$$

For the case of the solutes, the pressure terms in the equilibrium expression can be neglected since they are too small compared with the terms containing the solutes activities [27, 28]. These relations also apply to the other side of the membrane at the interface with the permeate stream (p). Consequently, the liquid inside the membrane pores can be regarded as a different phase, in which, due to the excluded volume near the pore wall, the solutes have a higher activity coefficient than in the surrounding aqueous phases and, therefore, a lower molar fraction [24]. Thus, φ can also be defined as the ratio between the activity coefficients at both sides of the interface (Eq. 12). Under diluted conditions, the value for the activity coefficient inside the pore γ_i' can be estimated from $\hat{\phi}_i$ as shown in Eq.13.

$$\varphi_i = \frac{x_i'}{x_i^w} = \frac{\gamma_i^w}{\gamma_i'} \tag{12}$$

$$\varphi_i = \left(\frac{\gamma_i^w}{\gamma_i'}\right); \quad diluted\ \gamma_i^w \approx 1 \ \therefore\ \gamma_i' = \frac{1}{\varphi_i} = \frac{1}{\hat{\phi}_i} \tag{13}$$

Many studies have reported that at concentrated conditions, the partitioning of a molecule in a non-adsorbing porous interface is not constant, but concentration-dependent [24, 29]. Even when solute molecules do not attract or repel each other, two mechanisms can still produce a change in the partitioning. The first mechanism is related with the fact that molecules always interact due to their mutual impenetrability. This short-range ordering effect gets more pronounced inside the pores due to the constriction [24, 30, 31]. The second mechanism refers to the interaction of the solutes with the solvent and its effect on the thermodynamics of the system. This last effect, in contrast, is more pronounced outside the membrane, where the concentration of solutes is higher, determining a higher value for γ_i^w than γ_i^p in the permeate [20]. Considering the fact that the membrane rejects most of the solutes, the solution inside the pores is assumed to be diluted. Therefore, only the second mechanism is considered in this study, alleviating the complexity in the calculations. Likewise, It is assumed that the value of $h_f = 3.8$ remains constant everywhere in the system. As consequence, unlike in diluted conditions, partition coefficients in concentrated conditions are expected to be different at both membrane interfaces (φ_w and φ_p at the interface with the retentate and permeate respectively).

2.3 Transport inside the membrane pores

To model the solutes transport through a NF/UF membrane a porewise approach can be used, in which it is assumed that pores are straight and cylindrical [2, 32]. This model has to be extended to consider the effect of osmotic pressure and the effect of high concentrations on the partition coefficients. Likewise, it has to consider the pore size distribution. Since the solution inside the pores is considered to be diluted, non-idealities and cross effects between solutes can be neglected. Therefore, γ_i' is

constant, and hence $\partial \ln \gamma_i' / \partial \ln x_i$ is zero and $\Gamma_i = 1$. The resulting binary Maxwell-Stefan Equation between species i and m (water) from Eq. 2 gets simplified as follows:

$$\frac{dx}{dz} + \frac{x_i \bar{v}_i}{RT}\frac{dP}{dz} = -\frac{x_i x_m (u_i - u_m)}{Đ_{im}} \tag{14}$$

We can work out Eq. 14 further by considering that at these conditions $x_m \approx 1$. $Đ_{im}$ should be corrected to calculate an effective diffusivity inside the pore $D_{p,i}$. Likewise, the solution velocity (approximated here to water velocity u_m) should also be corrected with a convection hindrance factor, K_c, to consider the flow inside the pore. The right hand side of Eq. 15 contain the terms that represent the three transport mechanisms for the solutes inside the membrane: convection, diffusion and the effect of the pressure gradient.

$$x_i u_i = K_c x_i u_m - D_{p,i}\frac{dx_i}{dz} - D_{p,i}\frac{x_i \bar{v}_i}{RT}\frac{dP}{dz} \tag{15}$$

After the inclusion of new variables such as Pe' and Y (see appendix C for the complete equation development), x_i can be integrated along the thickness of the membrane to obtain the following expression:

$$x_{i,p(r)} = \frac{\left(K_{c,i(r)} - Y_{i(r)}\right)\varphi_{w,i}\, x_{w,i}\, exp\left(Pe'_{i(r)}\right)}{\left(K_{c,i(r)} - Y_{i(r)}\right)\varphi_{p,i(r)} - 1 + exp\left(Pe'_{i(r)}\right)} \tag{16}$$

$x_{p,i(r)}$ is not the mole fraction of i in the permeate stream, but corresponds to the mole fraction of i just outside the membrane, at the permeate side, for only one specific pore size r as it is sketched in Figure 1A. This implies that the values of many variables of the model depend on the pore size. To calculate the overall concentration of i in the permeate stream $C_{p,i}$, the frequencies of the pore size distribution f_R should be considered as shown in Eq. 17 [32].

$$C_{p,i} = \frac{\int_0^{\infty} \frac{f_{R(r)}\, r^4\, C_{T,p(r)}\, x_{p,i(r)}\, \Delta P_{e(r)}}{\eta_{(r)}} \mathrm{d}r}{\int_0^{\infty} \frac{f_{R(r)}\, r^4\, \Delta P_{e(r)}}{\eta_{(r)}} \mathrm{d}r} \quad (17)$$

f_R is defined, assuming a log normal distribution, by two parameters: the mean radius r^* and the standard deviation σ (Eq. 18).

$$f_{R(r)} = \frac{1}{r\sqrt{2\pi b}} \exp\left\{ -\frac{\left[ln(r/r^*) + \frac{b}{2} \right]^2}{2b} \right\} \quad (18)$$

$$where\ b = \ln\left[1.0 + \left(\frac{\sigma^*}{r^*} \right)^2 \right]$$

It is important to emphasize that under concentrated conditions the pressure gradient is not similar to the effective pressure gradient ($\Delta P \neq \Delta P_e$). ΔP_e is a function of the osmotic pressure (Π), which counteracts the effect of ΔP as shown in Eq. 19 and in Figure 1B. Thus, on the one hand, the solutes transport due to the pressure gradient ΔP (3rd term in Eq. 15) is constant, while on the other hand, the convective transport of solutes is affected by the osmotic pressure generated due to the difference in the concentration of solutes at both sides of the membrane. Therefore, it is expected that the importance of the three different transport mechanisms inside the membrane changes depending on the feed concentration (Π_w and Π_p being the osmotic value on the feed side on the membrane surface and on the permeate side, respectively).

$$\Delta P_e = \Delta P - \Delta \Pi = \Delta P - (\Pi_w - \Pi_p) \quad (19)$$

A more accurate description of ΔP_e includes the so called Staverman reflection coefficient σ_v, resulting in the following expression: $\Delta P_e = \Delta P - \sigma_v \Delta \Pi$. σ_v can be calculated from the osmotic pressure values at both sides of both membrane interfaces as described by Bandini et al. [33]. For this study, however, this approach was not included to avoid increasing the complexity in the algorithm to solve the model. Thus σ_v is considered equal to 1.

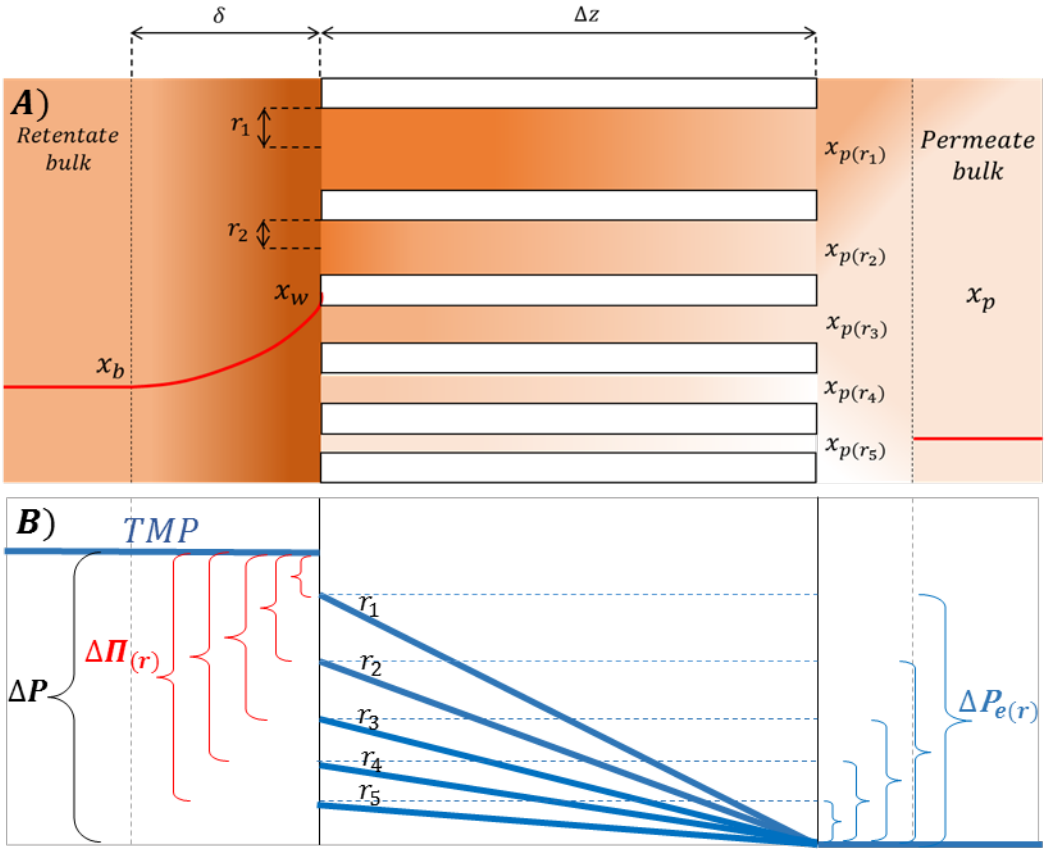

Figure 1. Schematic representation of the solute concentration (A) and the pressure profiles (B) over the UF system as described by the model. Both figures show the variables for different pore sizes.

As shown in Figure 1, the analysis presented here is for one particular pore, so independency between pores is assumed. At the permeate side of the pores, different compositions are expected depending on the pore diameter and, consequently, different osmotic pressure differences are generated over pores with different diameters. Larger osmotic pressures difference originates over smaller pores, resulting in a lower effective pressure.

To calculate $\Delta\Pi$, it is necessary to know the composition at the membrane and permeate sides of every pore size. These compositions yield the water activity (a_{H2O}) using Eq. 20, which has been derived in detail in the appendix D. The osmotic pressure compared to pure water Π can then be calculated using Eq. 21 [21].

$$a_{H2O} = \frac{x_{H2O} - h_f x_{seg}}{1 - h_f x_{seg}} \tag{20}$$

$$\Pi = -\frac{RT}{\bar{v}_{H2O}} \ln a_{H2O} \tag{21}$$

2.4 Flux calculation

Apart from the modelling of the permeate concentration, the calculation of the flux should also be included in the model. As can be seen in Eq.3, to solve x_i along the concentration polarization layer, the solute fluxes (N_i) must be known. An extra relationship, known as 'bootstrap', linking the fluxes and the molar fractions, is needed to solve the system of Maxwell-Stefan Equations [16]. Eq. 22 can be used for this purpose.

$$N_i = x_i N_T \tag{22}$$

To calculate the total molar flux (N_T), Eq. 23 can be used, for which the value of the total volumetric flux (J_v) is needed. As shown in Eq. 24 , J_v cannot be calculated in advance because it is a strong function of the pore-dependent effective pressure $\Delta P_{e(r)}$ [32]. As consequence, an iterative procedure is required to solve J_v starting from an educated guess.

$$N_T = J_v \, C_{T,p} \tag{23}$$

$$J_v = P_n \, \pi \int_0^\infty f_{R(r)} \, V_{(r)} \, r^2 \, dr = \left(\frac{P_n}{\Delta z}\right) \frac{\pi}{8} \int_0^\infty \frac{f_{R(r)} \; r^4 \, \Delta P_{e(r)}}{\eta_{(r)}} dr \tag{24}$$

J_v also depends on two unknown parameters: The number of pores per square meter of membrane surface area (P_n) and the thickness of the active layer of the membrane (Δz) [32]. Nevertheless, these two parameters can be conveniently lumped in one: $\frac{P_n}{\Delta z}$. This is a geometric parameter (constant) of the

membrane that, when the membrane pore size distribution is known, can be calculated from experimental data using the pure water flux.

3. MATERIALS AND METHODS

3.1 Chemicals

Demineralised water was used in every experiment. The fructo-oligosaccharides mixture Frutalose® L85 (batch: 8554908001) was kindly provided by Sensus (Roosendaal, The Netherlands). This mixture is a viscous, clear syrup with a concentration of 75°Brix, composed of mono, di and oligo-saccharides with DP up to 10. Its composition on dry basis is shown in Table 1.

Table 1. Composition on dry basis of fructooligosaccharides mixture (Frutalose® L85) and other properties of the sugars at 45°C.

Component	% [w/w]	D_i^{∞} [10^{-10} m^2/s]	$\overline{v}_i$ (10^{-4} m^3/mol)	r_G^* (10^{-10}m)
DP1	6.1	10.05	1.79	4.14
DP2	7.6	8.13	3.03	5.99
DP3	28.8	7.16	4.36	7.85
DP4	22.5	6.53	5.64	9.70
DP5	16.9	6.08	6.92	11.55
DP6	12.2	5.73	8.20	13.40
DP7	5.9	5.45	9.49	15.26

DP = Degree of polymerization, * average radius calculated according to our previous study [13].

3.2 Membrane

A thin film composite (thin polyamide layer deposited on top of polysulfone porous layer), spiral wound GE membrane (GE Osmonics, Sterlitech, Kent – WA, United States) was used for all the experiments. The pore size distribution of this fine ultrafiltration membrane was determined in our previous study by doing a fitting procedure using experimental rejection data obtained under diluted conditions [13], and the lumped parameter $\frac{P_n}{\Delta z}$ was estimated to be 1.53x10^{13} pores/m^3 using Eq. 24. These, among other membrane specifications, are shown in Table 2. The experiments were performed in a pilot scale filtration system that included heat exchangers in the feed tank and in the recirculation loop of the retentate. The flow, temperature, brix and pressure of both retentate and permeate streams were monitored by computer (using DDE software from Labview).

Table 2. Specifications of GE membrane

Membrane specifications	**GE**
Model	1812C-34D
Type	Spiral wound
Manufacturer	General Electric
Membrane material	TFM
MWCO (declared by manufacturer)	1000 Da
Membrane area	0.32 m^2
Spacer height*	8.60 x 10^{-4} m
Spacer porosity*	0.93
Maximum temperature	50°C
Pore size distribution [13]*	r^*=1.29nm, σ= 0.17
$P_n/\Delta Z$*	1.53x10^{13} pores/m^3

*Membrane characteristics measured in our lab.

3.3 Experiments at high concentrations

Experiments using the fructooligosaccharides mixture at different concentrations (0.5% - 35% w/w) were performed using the GE membrane. The retentate and permeate streams were recycled back to the feed tank, and once the system reached steady state (constant permeate flux and Brix), samples were taken from both streams simultaneously. Table 3 summarizes the process conditions for all the experiments. All runs were performed at 45°C to mimic industrial conditions and to avoid microbial

growth. The retentate recirculation flow was 150 L/h with a crossflow velocity of 0.088 m/s in the membrane module.

Table 3. Experimental process conditions

Concentration %(w/w)	Pressure [bar]
0.5%	2.5, 7.5, 10, 12.5, 15, 17.5, 20.
5%	8, 12, 16, 20, 24.
10%	20.
20%	10, 12, 14, 16, 18, 20, 22.
25%	12, 14, 16, 18, 20, 22.
30%	20.
35%	16, 20, 24

*All the transmembrane pressures declared in this study are the resulting average along the membrane TMP= (P_{inlet} + P_{outlet})/2.

3.4 Model assumptions

The complexity of the multicomponent concentrated system was alleviated by key assumptions that enable the resolution of the model.

- In the concentration polarization layer, a uniform layer thickness (δ) was used for the integration of the molar fraction of all the solutes [14]. As the concentration profiles of larger solutes are steeper than those of small solutes, modelling the transport of the larger solutes is more sensitive to δ. Therefore, δ was calculated (Eqs. A1-A4) using the diffusivity of the largest solute in our mixture (DP7).
- Since inside the membrane the concentration of solutes is low (most of them are retained by the membrane), the value calculated for γ_i' using Eq. 13 was considered constant along the length of the pores. In other words, only the excluded volume due to the pore wall was considered in the calculation of γ_i', while the effects of hydration were neglected. Conversely, the values of γ_i^w and

γ_i^p were calculated considering the effect of hydration according to their local composition using Eq. 6.

- The concentrations of the solutes just before the membrane $C_{w,i}$ were assumed similar for all pore sizes, as sketched in Figure 1. Transversal diffusion and even convection over the membrane surface ensure that local differences are evened out. The effect of different pore sizes is reflected only in the mole fraction inside the pores $x_{i(r)}$ and in the permeate just outside the pore $x_{p,i(r)}$.

3.5 Prediction of the permeate flux and permeate concentrations (algorithm)

The model was created using the equations given in section 2 and the aforementioned assumptions. The model inputs are the process conditions (solutes concentrations in the retentate and the applied TMP), the membrane pore size distribution and the structural membrane parameter $\frac{P_n}{\Delta z}$ (Eq. 24). Figure 2 shows the algorithm for the resolution of the model.

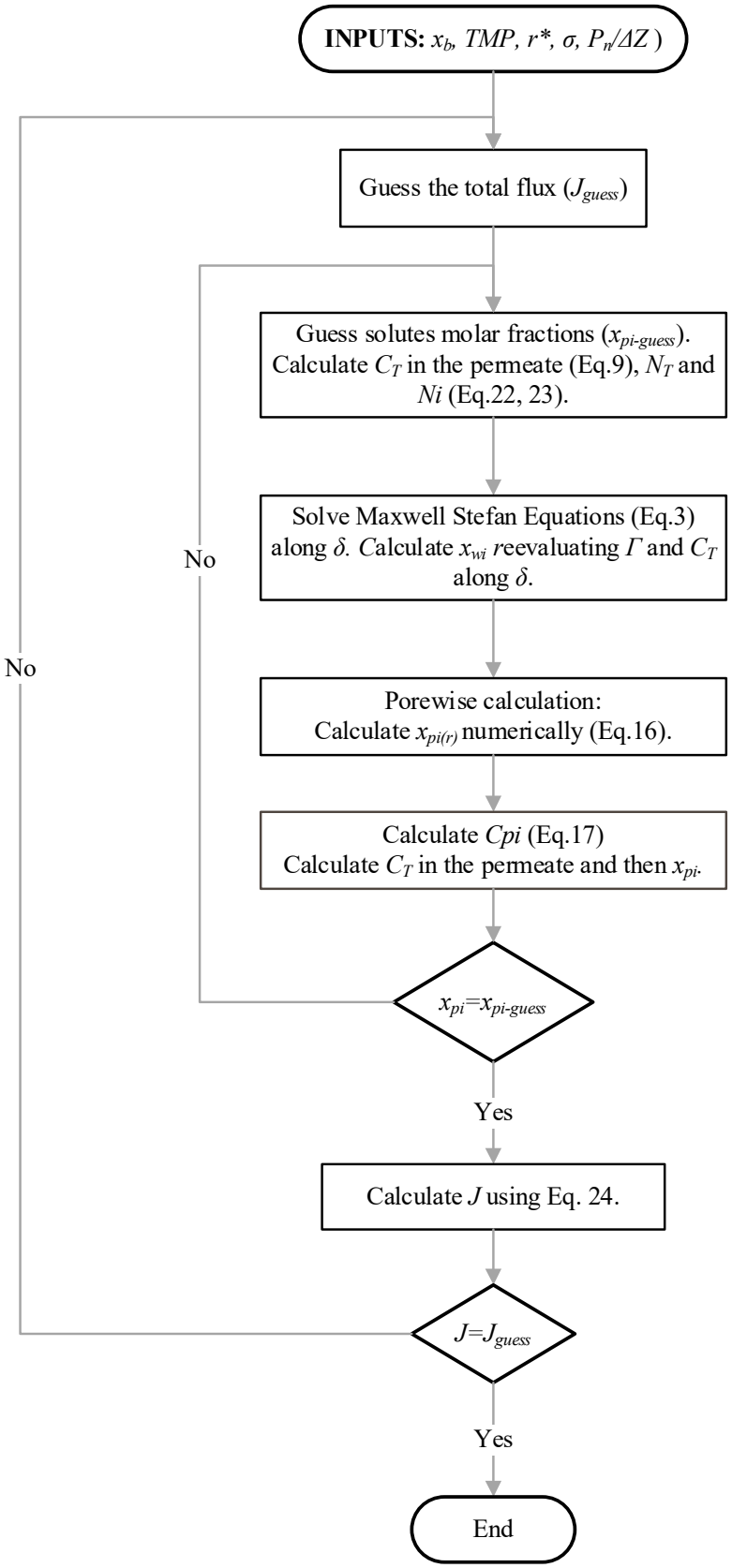

Figure 2. Algorithm for the resolution of the multicomponent model for concentrated conditions.

3.6 Analytical methods

The concentration of the different sugars in the oligosaccharides mixture was measured using ion exchange chromatography, using a method based on the study of Campbel et al. (1997) [34]. The Dionex column Carbopac PA-100, 250 x4.6mm + guard was employed at 20ºC. Three eluents were used: Demineralised water, 0.25M NaOH and 0.65M NaOAc at a flow rate of 1mL/min. The detection was performed with an electrochemical detector (Dionex ED-40, range 500 nC, pulse train 2).

3.7 Computational analysis

MATLAB R2017b was used for all the calculations. Numerical integrations were performed using the function 'integral'. The numerical procedure to find J_v and x_{pi} was done with the function 'fsolve', which is a solver for systems of non-linear equations that uses the 'trust-region-dogleg' algorithm. To solve the Maxwell Stefan equations, the function ode15i was used, which allows to solve systems of implicit differential equations.

4. RESULTS AND DISCUSSION

Experiments with the oligosaccharide mixture up to a feed concentration of 35% (w/w) were performed at different TMPs. It was found that, for each pressure, the observed rejection of all the solutes decreased (especially DP1-2) as the concentration in the feed increased. At feed concentration of 20% w/w and higher, negative values were observed for DP1 sugars. Figure 3 shows a comparison of the observed rejection as a function of applied TMP at different feed concentrations. The decrease in the observed rejection of solutes was more notorious for the smaller molecules DP1 and DP2 up to a concentration of 25%. At 35%, there was a pronounced decrease in the observed rejection of the bigger molecules of the mixture, while the values for DP1 molecules remained stable. The complete experimental data set can be found as Supplementary Material.

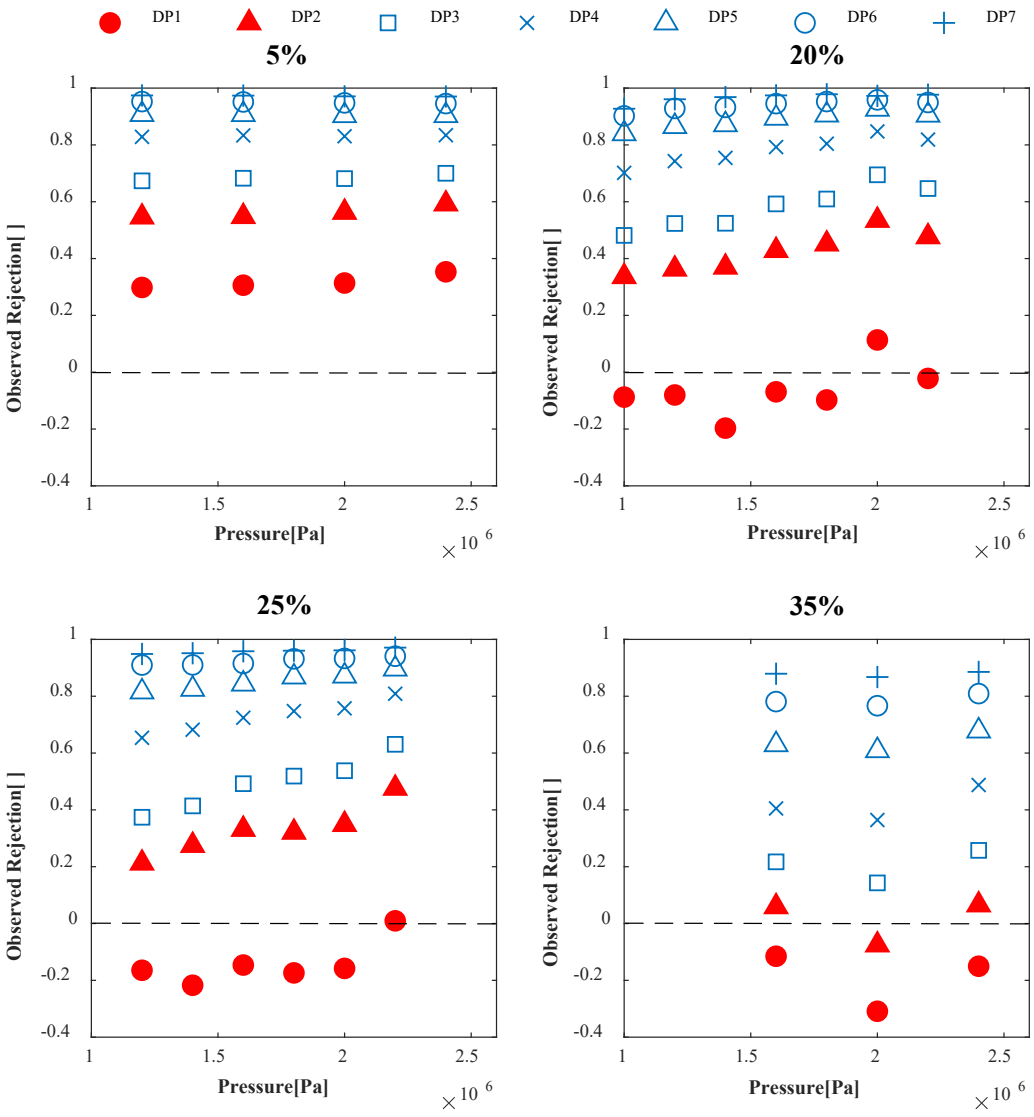

Figure 3 Observed rejection as function of pressure for fine UF experiments at feed concentrations 5, 20, 25 and 35% w/w. The rest of the process conditions were similar in all experiments (crossflow velocity =0.088m/s, T=45°C). The concentration units used for the calculation of the observed rejection were g/kg.

The observation of negative rejections has been ascribed to different effects [9, 35].

(1) Negative rejections have been linked by some authors to selective ionic transport and electrical interactions with the membrane [36]. In our case, we ruled out the possibility of electrical interactions because only neutral solutes are used in this study.

(2) Likewise, we consider membrane adsorption and fouling unlikely due to the flux stability over time, which is supported by the complete recovery of the original water permeability after a short rinsing step.

(3) We also made sure that the reduction in the observed rejection was not produced merely by the decrease in permeate flux at high concentrations, by comparing experiments with similar permeate flux. Figure 4 shows that the reduction in hydrodynamic drag, produced by the permeate flux decrease, cannot explain the magnitude of the reduction in observed rejection of DP1 molecules.

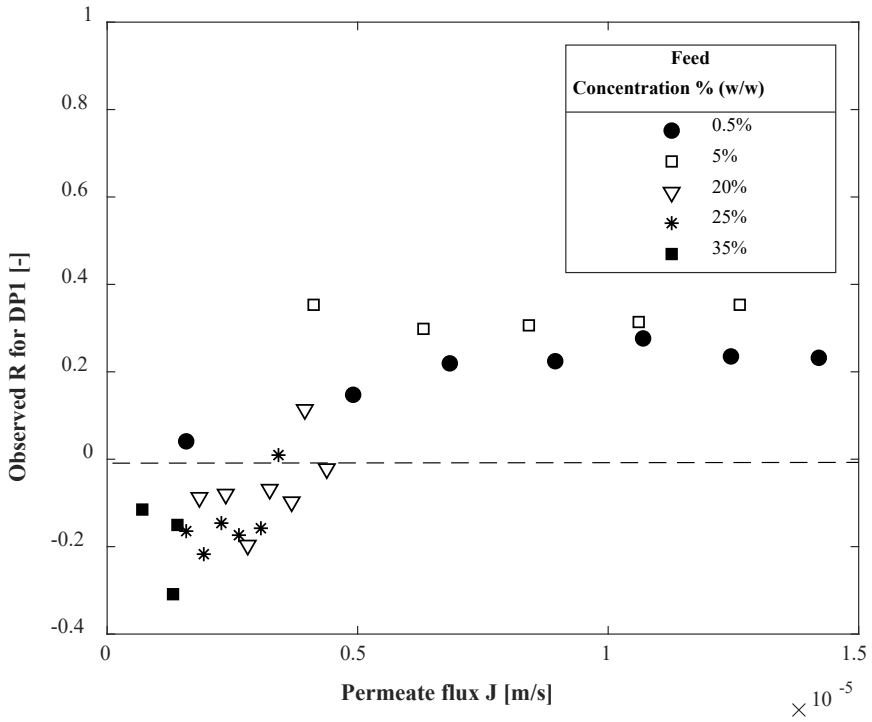

Figure 4. Observed rejection of DP1 molecules at different feed concentrations as function of permeate flux (J).

In order to check whether the changes in the thermodynamics of the system due to high concentrations can explain the decrease of the observed rejections, a model that considers the change in the solutes chemical activities was built. As described in sections 2.1-2.3, hydration effects and a porewise representation of the conditions inside the membrane were incorporated in our model. Figure 5 shows

the comparison between the permeate concentrations predicted by our model and the measurements from experiments under different process conditions. The match is satisfactory especially for the smaller molecules (DP1-DP4) and becomes less accurate at very high permeate concentrations. For the bigger molecules (DP5 - DP7) for which the observed rejection is almost 1, some deviations can be noticed in the lower part of the graph. At high feed concentration, the model predicts higher concentrations in the permeate than in the retentate for DP1 and DP2. This goes in line with the negative observed rejections obtained experimentally for these molecules. Further discussion on the relevant mechanisms that make these predictions possible is presented in the next sections.

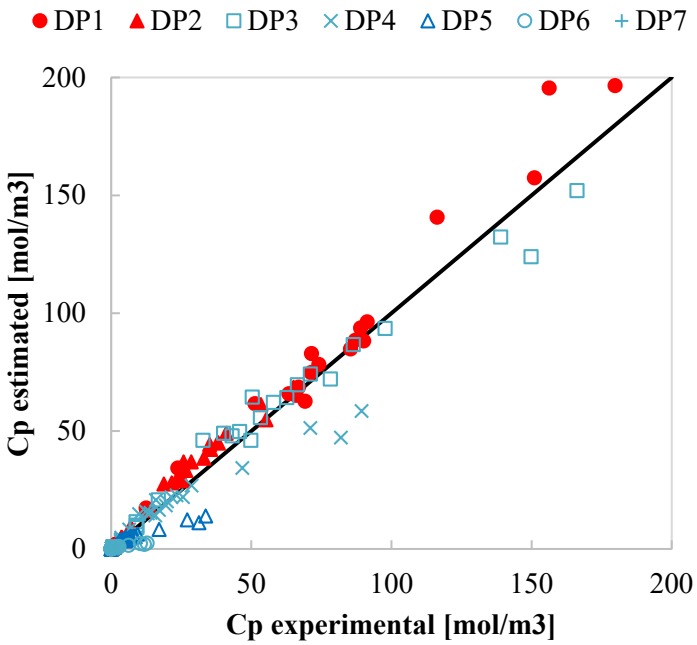

Figure 5. Comparison between estimated and experimental data on permeate concentration.

4.1 Thermodynamic effects

At the sugar concentrations used in this study, hydration is the most relevant thermodynamic phenomenon [11, 19, 20]. The strong interaction between the hydroxyl groups of the sugar molecules and water molecules 'removes' free water from the solution, increasing the chemical activity (a) of the water. Therefore, less water is available for other solutes, which also increases their activity. This translate to an increase in the activity coefficient, considering that $a_i = x_i \gamma_i$. Since the hydration of all

sugar segments is assumed to be the same, as was discussed in section 2.1.1, the value of the activity coefficient of all solutes has to be the same.

Figure 6 shows the results obtained by solving the Maxwell Stefan Equations in the concentration polarization layer, in which the activity coefficient increases along the layer thickness due to the increment in the concentration of solutes. The value of γ increases from 1.13 to 1.18 over a layer thickness of 56μm. It is important to notice that γ is not equal to 1 at the point δ=0 since the effect of hydration is already relevant at the concentration in the bulk of the retentate (≈ 25%w/w).

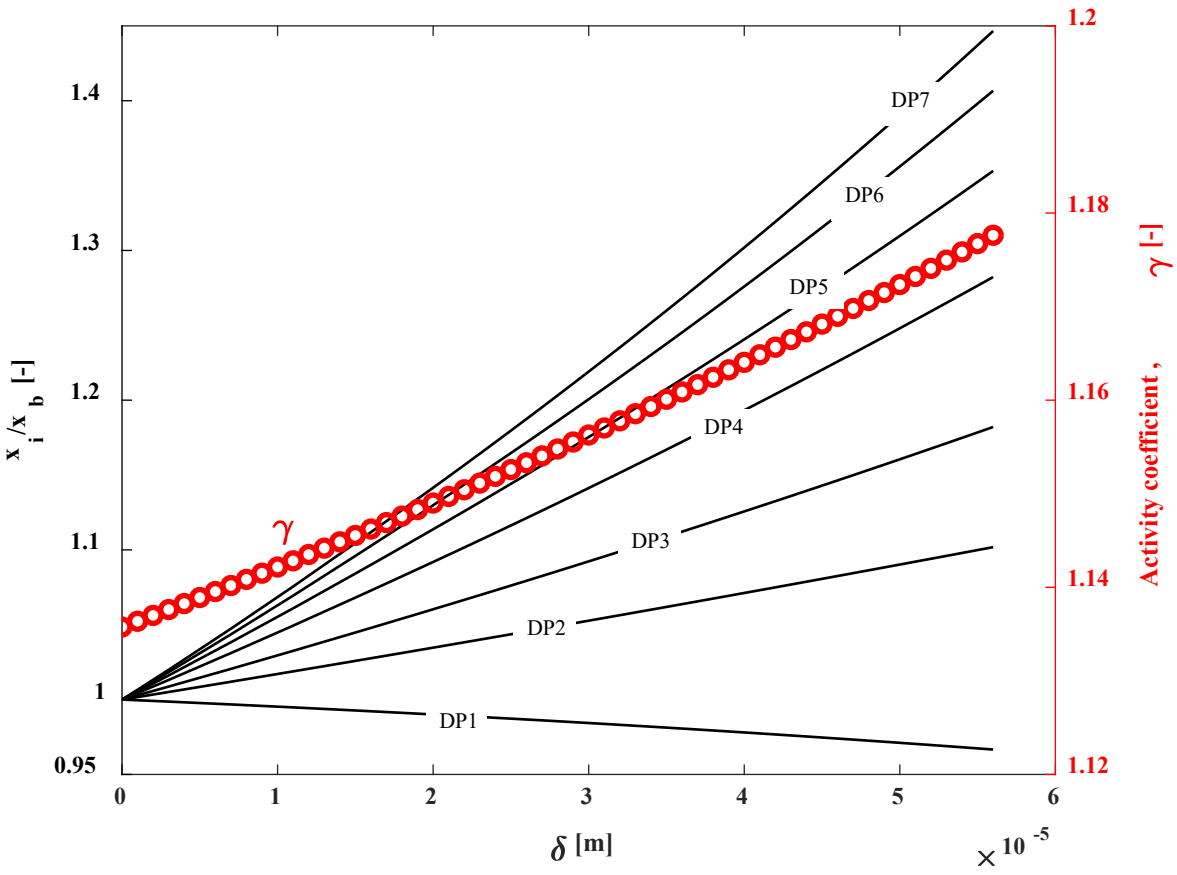

Figure 6. Concentration profiles and solutes activity coefficient along the thickness of the concentration polarization layer. Prediction corresponds to the following process conditions: 25% w/w and TMP = 20 bar.

The effect of hydration becomes more important at the membrane interface, which is relevant for the partitioning of the solutes. As shown in Eq. 11, at local thermodynamic equilibrium, the activity of the solutes at both sides of the interface must be the same ($x_i^w \gamma^w = x_i' \gamma_i'$). Since the concentration of solutes inside the pores of the membrane is low, γ_i' remains constant and not affected by the 'external conditions'. As consequence, an increment of γ^w causes an increment in x_i', and thus a higher partition coefficient. As γ^w is the same for all the solutes, this increment of the partition is proportionally similar for all the solutes. Nevertheless, the increment it is larger for the smaller solutes since they have a lower activity coefficient γ_i' inside the pores (see Eq. 13). Figure 7 shows how the partition coefficient of a DP1 molecule depends on the feed concentration and on the pore size. The effect of high concentration is more notorious in the larger pores because there γ_1' is lower. We must keep in mind, however, that the solute concentration in these pores is larger than in the smaller pores, and therefore our assumption of a constant γ' in these larger pores is less accurate at concentrated conditions [24, 29].

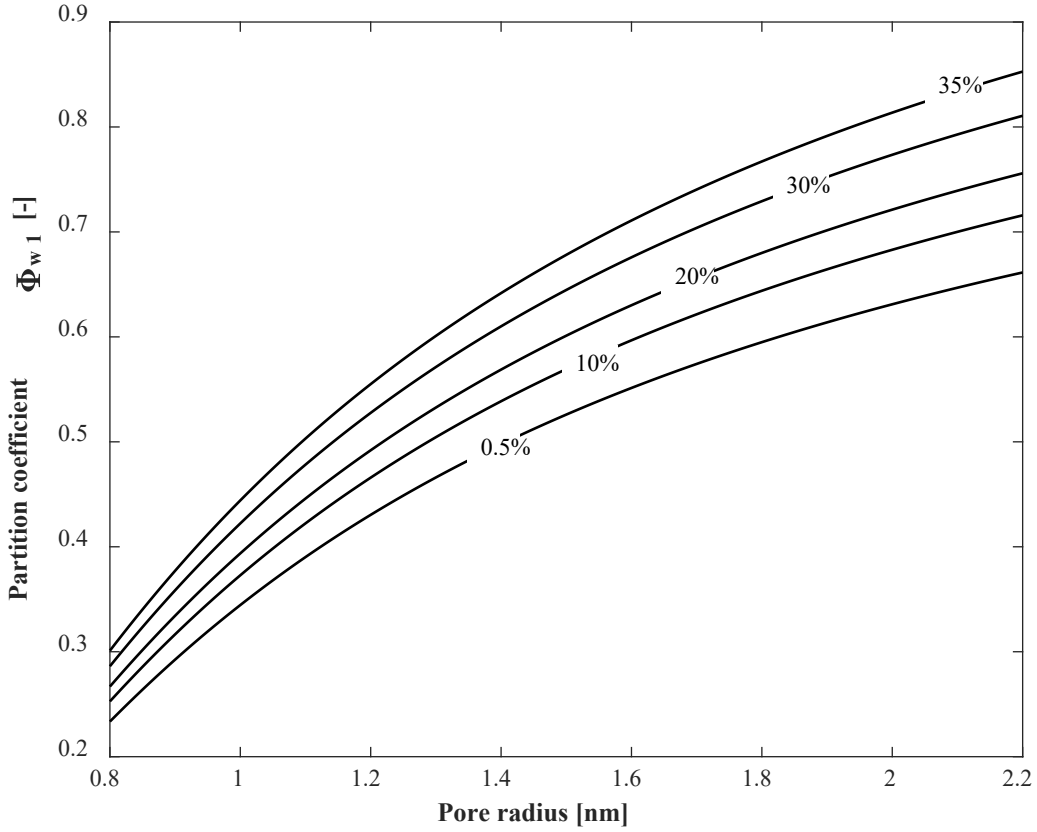

Figure 7. Partition coefficient of DP1 molecules at the interface between the retentate and the membrane. $\boldsymbol{\varphi_{w1}}$ is presented as a function of pore size for different retentate concentrations. These predictions were generated by our model using a TMP of 20 bar.

By using our model, activities and molar fractions can be calculated at any point in the system. These two variables for a DP1 molecule were compared under diluted and concentrated conditions (Figure 8). In the case of a diluted feed, the activity and the molar fractions have the same value, since it is thermodynamically ideal ($\gamma \approx 1$ in the feed and permeate). Thus, there is no interaction between the solutes due to hydration, and the solute fluxes are independent of each other.

On the other hand, at high concentrations, because of the hydration phenomena, the activity increases, reaching its maximum at the membrane surface (at the retentate side). Under these conditions, something noteworthy occurs in the concentration polarization layer: The molar fraction and the activity gradient for DP1 have different sign. This is only possible because of the presence of other solutes that bind water, thus making water less available near the membrane. Darken and other authors

have reported this type of situations in complete different of systems (e.g. diffusion of carbon in austenite bars) [37-39]. They agreed in the importance of considering the chemical potential gradient as the truly driving force for diffusion.

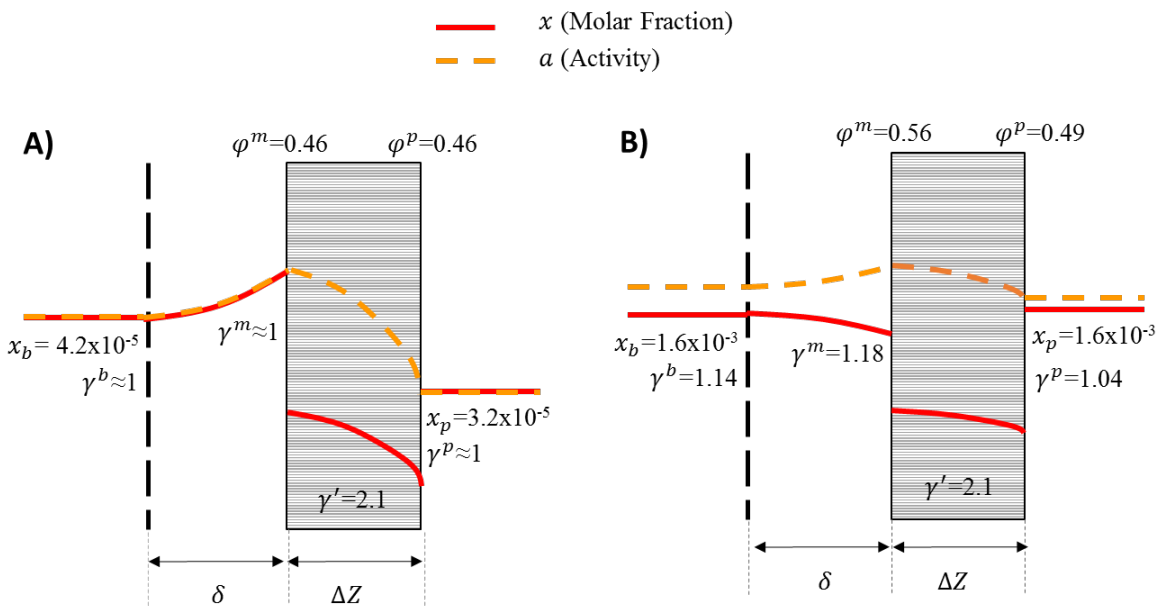

Figure 8. Concentration and activity profiles for DP1 over the UF system at diluted (A) and concentrated conditions (B). The feed concentration in was 0.5% w/w in A and 35% w/w in B. The rest of the process parameters were similar (TMP=20 bar, 45ºC).

At concentrated conditions, the partition coefficients are different at both sides of the membrane. Since γ^w is higher than γ^p, and γ' is constant, a higher φ value originates at the membrane interface that is in contact with the concentrated phase. Additionally, the molar fractions of DP1 were similar in the retentate and permeate, determining an observed rejection of zero. The same value calculated with concentration units g/kg was around -0.3 due to the difference in C_T in the permeate and retentate stream. Finally, it is also remarkable in Figure 8 the different way how the concentration profiles evolve along the membrane, even when, for modelling purposes, no thermodynamic considerations were made inside the membrane pores. This is discussed further in the next sections.

4.2 Pore size distribution effects.

Apart from the hydration effects, the model allows us to analyse the effects of the pore size distribution in concentrated systems. Figure 7 illustrates that some variables inside the model vary depending on the pore size. This brings up the question about the importance of the distribution of pore sizes under concentrated conditions.

Figure 9 shows the pore size distribution based not in the pore size but on the volumetric flux through the pores. This calculation was made using a $\frac{P_n}{\Delta z}$ value of 1.53×10^{13} pores/m^3, which we estimated from flux measurements using pure water. The overall flux decreases as the concentration of the feed goes up. This decrease is, however, not similar for every pore size, but more prominent for smaller pores because the difference in osmotic pressure over these pores is larger than that over bigger pores, as illustrated in Figure 1. Therefore, the shape of the distribution get slightly skewed to the left, increasing the importance of the transport through the biggest pores.

The volumetric flux (J_v) is a very strong function of the pore radius (Eq. 24), which means that the big pores are dominant in the overall separation. This can also be seen by comparing the mean radius under different circumstances. The mean radius r^*, based on the number of pores (frequencies), is 1.29 nm. For the same membrane the mean radius based on the volumetric flux is 1.39 nm at a retentate concentration of 0.5% and 1.46 nm at 35% w/w. Therefore, under concentrated conditions, the transport through the bigger pores becomes even more important, which causes the rejection of all solutes to decrease since the larger pores impose less size exclusion.

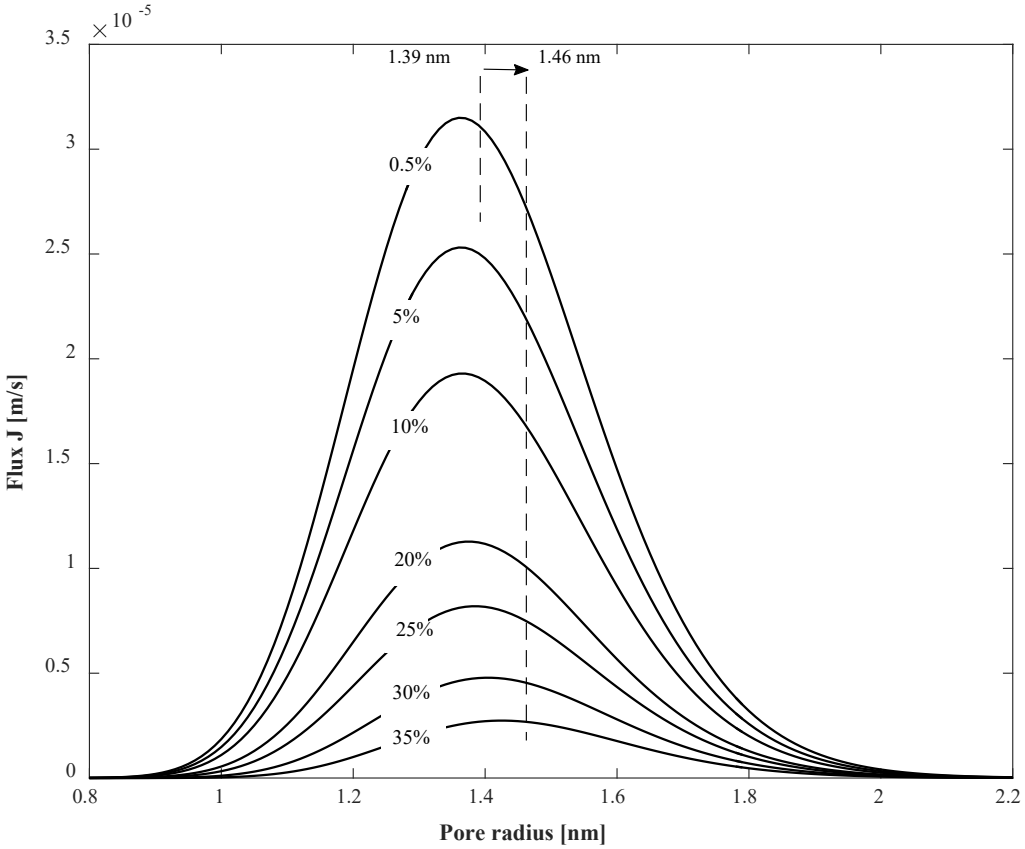

Figure 9. Pore size distribution based on the porewise volumetric flux at a TMP of 20 bar. Dashed lines represent the mean pore size for the distributions at a feed concentration of 0.5% and 35% w/w.

The predictions for J_v were calculated by integrating the porewise volumetric flux curves (Eq. 24), such as the ones shown in Figure 9. A very good match between the experimental data and predictions were found for all the performed experiments (Figure 10). As expected, higher accuracy was obtained at diluted conditions were the effects of osmotic pressure and increased viscosity are still not relevant. At higher concentrations, the model tends to slightly overestimates the flux, probably due to the small overestimation of the permeate concentrations (Figure 5), which increases the effective pressure over the membrane. Consequently, even better predictions may be attained if hydration effects inside the membrane would be considered. These effects would increase the value of γ_i', reducing the concentration of solutes inside the membrane and in the permeate.

It was not experimentally feasible to perform experiments at retentate concentrations higher than 35%w/w with a TMP of 20 bar since the obtained fluxes were too small to be accurately measured. Similarly, model-wise, it was not possible to obtain predictions at higher concentrations since the obtained porewise volumetric fluxes were negative for narrow pore sizes and convergence was not attained using our algorithm.

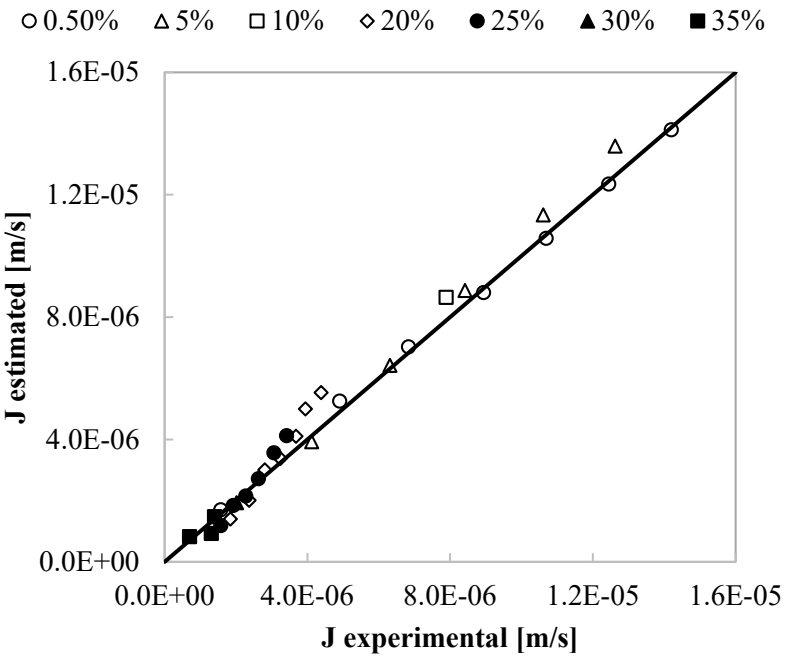

Figure 10. Comparison between experimental and modelled volumetric flux $\boldsymbol{J_v}$ at different experimental conditions.

In addition to C_p and J_v, it is possible to obtain an estimation of the membrane porosity (ε) if the thickness of the active layer of the membrane ΔZ is known. As a rough estimation, we can assume a ΔZ of 1μm, which is a value often reported in literature [1, 2]. The number of pores (P_n) can be estimated from the $\frac{P_n}{\Delta z}$ value and ε can then be calculated using P_n and the frequencies of the pore size distribution, as follows:

$$\varepsilon = P_n \pi \int_0^\infty f_{R(r)} r^2 \, dr \tag{25}$$

The obtained value for ε was 0.026, which is in the same order of magnitude as other reported values [1, 2, 40]. This demonstrates the consistency of our model since it can represent flux and rejection while keeping the physical properties of the membrane within the expected order of magnitude. It also indicates that the assumption of independency among pores is likely to be true with such small porosity.

4.3 Transport mechanisms inside the pores

The relative importance of the solute transport mechanisms inside the membrane depends on the solutes concentration (Eq.15). At diluted conditions, convection and diffusion due to a concentration gradient are the main transport mechanisms, while the effect of TMP over the diffusion of the solutes is small and often neglected [2, 33]. However, at concentrated conditions, the reduction of the effective pressure due to the osmotic pressure, reduces largely the convection through the pores. As consequence, the solute transport driven by the gradients in the system (concentration and pressure) becomes more important. It is critical to notice that even when the effective pressure over the system has diminished, the TMP, which is the pressure driving force over the solutes, remained the same.

Figure 11 shows the effects of high feed concentrations on the concentration profiles inside the membrane pores. Normalized profiles are shown with and without considering the effect of the pressure gradient on the solute concentrations. Under diluted conditions, the effect of including the pressure gradient is negligible; however, under concentrated conditions it becomes quite important, increasing the transport of solutes towards the permeate. This is in line with the observations by Van Oers et al., who considered the reduction in the observed rejection of PEG3400 in the presence of dextran more related to the TMP than to the permeate flux [9].

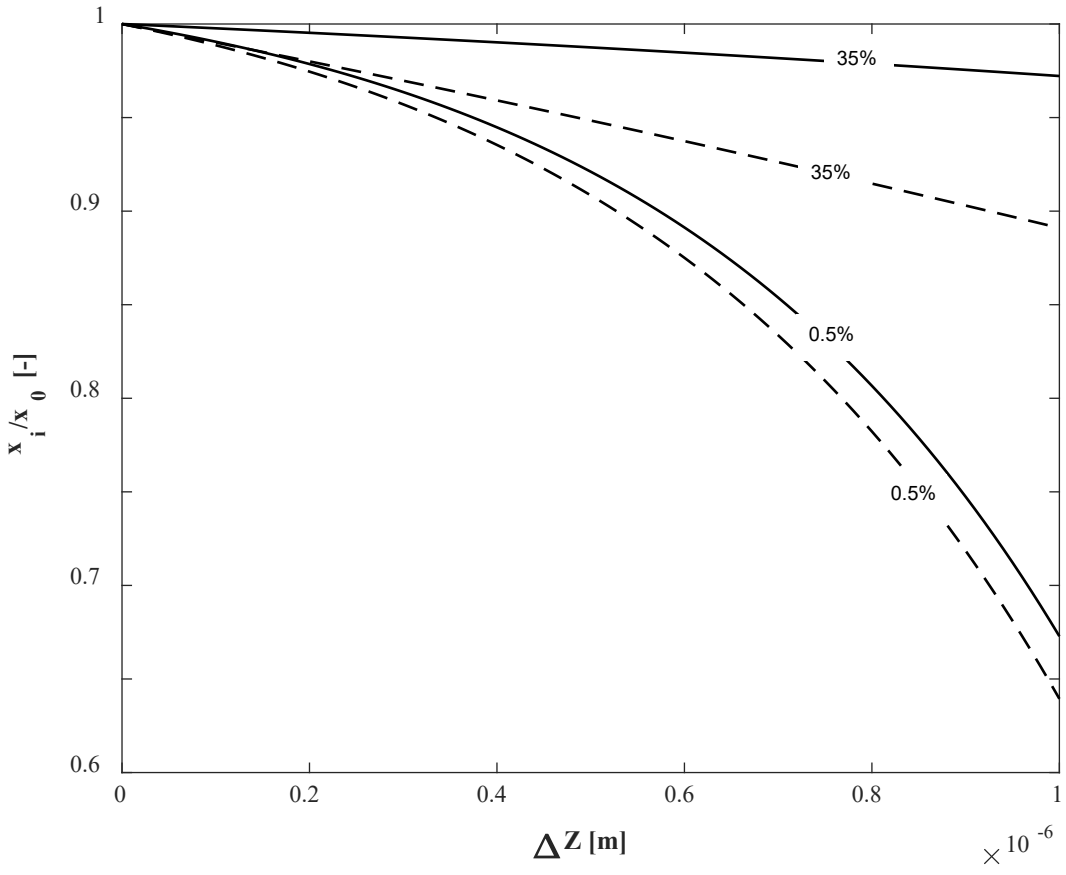

Figure 11. Normalized concentration profiles along the pore length for DP1 molecules under diluted and concentrated retentate conditions. The shown profiles correspond to a pore with $\boldsymbol{r_p}$=1.29 nm using TMP= 20 bar. Continuous lines represent the complete model and the dashed lines correspond to the model without the contribution of the pressure gradient ($\boldsymbol{Y}$=0 in Eq. 16).

As previously discussed, larger feed concentrations reduce the importance of convective flow in the transport of solutes, relative to the effects of diffusion due to the concentration and pressure gradient. To establish whether the rejection of small solutes gets more reduced by this effect than that of bigger solutes is necessary to look back to Eq. 15. Here the importance of the pressure gradient is co-determined by the product of the diffusion coefficient and the molar volume of the solute, $D_{p,i}\overline{v}_i$, which depends both on the pore size (exclusion) and on the molecular weight of the solute. While the bulk diffusion coefficient increases only slightly on the molecular weight, it decreases strongly when the size of the solute come in the range of the pore size, due to exclusion effects. Combined with the effect of the molar volume $\bar{v}_i$, which is roughly proportional to the molecular weight, we see that

$D_{p,i}\overline{v}_i$ increases with the molecular weight in larger pores (due to $\overline{v}_i$), but decreases with the molecular weight in small pores (due to the exclusion factor $K_{d,i}$) (Figure 12).

This explains the observed changes in the solutes rejection in Figure 3. At moderate concentrations (20-25%w/w), the observed rejection of DP1 molecules is markedly lower than with dilute concentrations, with almost no difference in the values for the biggest molecules (DP6-7). On the other hand, at high concentrations (35%w/w), the mean pore size shifts towards the right, and the observed rejection of DP1 molecules decreases slightly, while that of the biggest molecules decreases more strongly.

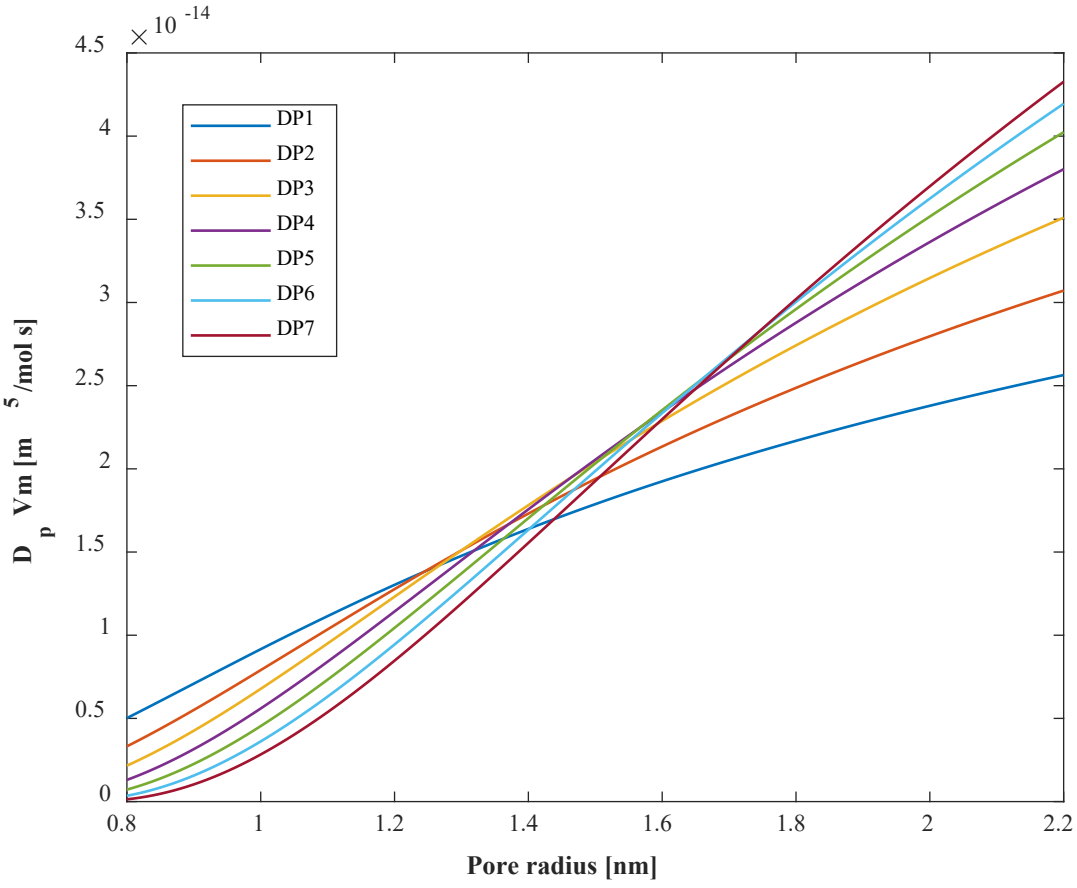

Figure 12. Product of $\boldsymbol{D_{pi}}$ and $\boldsymbol{V_i}$ for all solutes at different pore radii. Values were estimated considering a retentate concentration of 25%w/w and TMP=20 bar.

4.4 Process optimization

The changes in the observed rejection for the different sugars suggest that there is an optimum feed concentration that gives the highest efficiency for the removal of DP1-2 molecules. This optimum concentration was identified in Figure 13(top), in which the purity of the DP1-2 molecules in the permeate stream is shown as function of the feed concentration. Likewise, the mass flux of these two molecules is shown in the figure to complete the analysis of the effect of feed concentration on the process efficiency.

The maximum efficiency was found at a retentate concentration of approximately 25% w/w. Although higher purity can be obtained at a feed concentration of 0.5%, this concentration is not convenient due to the low mass flux. Interestingly, the enhancing effect in the transport of large molecules due to the pressure gradient at very high concentrations, resulted in a marked decrease in the permeate purity of DP1-2. Notice that the optimum concentration depends on the membrane, since all the results depends strongly on the pore size distribution.

Figure 13 (bottom) shows the reduction in the observed rejection of the molecules as the concentration in the retentate gets higher. In the case of the bigger molecules, the reduction in observed rejection becomes significant at a concentration of 20% w/w, and from there it decreases quickly with concentration. For the smaller molecules (DP1-DP2), this effect is more noticeable at lower concentrations and it is reaching negative values at feed concentrations higher than 20%.

The importance of the thermodynamic effects at high concentrations was evaluated by comparing the predictions of two models. The continuous lines represent the full model as described in this study, while the dotted lines represent the same model without the inclusion of the thermodynamic effects, by using constant activity coefficients ($h_f = 0$). It can be seen that at feed concentrations of 25% w/w, the estimated rejections for both models deviate considerably from each other, being always the prediction with the full model lower than that of the simplified model.

Due to the dispersion of the experimental measurements, however, we cannot distinguish between the accuracy of both models. It seems that the simplified model is good enough at moderate

concentrations up to approximately 30%w/w, because at 35%, it overestimates the rejection of all the solutes with a root-mean-square deviation (RMSD) of 0.19, while a better prediction (RMSD=0.14) is obtained with the full model. These observations, of course, depend on the membrane and on the size of the neutral solutes, so it is difficult to generalize. In filtration systems with bigger solutes or smaller membrane pores, the effect of concentration is expected to be relevant at lower feed concentrations than what we observed in this study.

The simplified model does not consider the thermodynamic effects at high concentration, but it does consider all the other effects described in this study (pore size distribution effects, pressure effects and the intermolecular friction calculated with the Maxwell-Stefan equations). These other effects also lower the rejection of solutes at high concentrations but not as sharply as when the change in the activity coefficients is considered. Both models are able to describe negative rejections for small molecules, and are certainly more effective on describing the reduction on the observed rejection for the small molecules than for the big ones, for which their rejections are constantly overestimated. The reason might be related with the alignment of elongated molecules inside the pore, which is an effect that was not considered in our study [13]. At diluted conditions, this omission is not important but under concentrated conditions molecular alignment due to steric interactions might be occurring inside the pores.

In general, the accuracy of the models can still be improved. We believe that two sources of inaccuracy are the assumption of diluted conditions inside the membrane at very high feed concentrations (higher than 30%w/w) and the fact that we did not include Staverman coefficients during the effective pressure gradient (ΔP_e) calculation. Including these two aspects demands much more computational resources to solve the model. For simpler systems with less components, however, it is a plausible option.

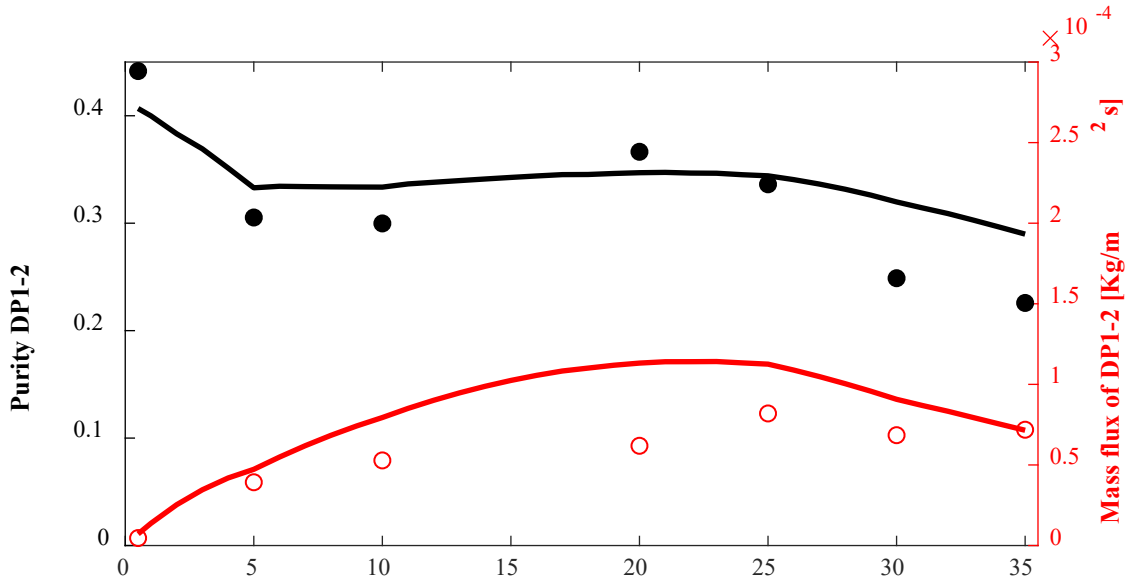

Figure 13. Top: Model estimations of Purity (black line) and mass flux (red line) of DP1-2 molecules as function of feed concentration. Bottom: Model predictions of the observed rejection as function of feed concentration using $\boldsymbol{h_f}$=3.8 (continuous line) and using $\boldsymbol{h_f}$=0 (dotted line). Markers represent experimental measurements, which correspond to experiments performed at 20 bar.

5. CONCLUSIONS

The effect of high solutes concentration in fine UF was studied using a mixture of oligosaccharides with a feed concentration up to 35% w/w. A model was created that included the non-ideality of concentrated sugar solutions, pore size distribution and pressure effects.

The observed rejection of all solutes decreased as the concentration in the feed increased. For the smallest solutes negative retentions were observed. The reasons of such behaviour are not because of ionic interaction or membrane adsorption or fouling, but are mainly due to pore size distribution effects and the non-ideality of concentrated sugar solutions.

Due to hydration, the activity coefficient of the solutes increases at high concentrations. This influences the driving force for diffusion in the concentration polarization layer. Additionally, at the membrane interface, the local equilibrium of one concentrated phase (retentate) and one diluted phase (membrane pore), enhances the transport of small solutes inside the membrane.

The difference in the osmotic pressure is larger over narrow pores than over large ones. As consequence, higher concentrations reduce more strongly the flux through narrower pores, increasing the importance of the transport through the larger pores. Additionally, solute transport due to the pressure gradient, normally neglected in most of the studies, becomes important at high concentrations, at which convective transport is lowered due to the osmotic pressure effects.

The results show that for a particular membrane, there is an optimum concentration for obtaining the highest efficiency in the removal of small sugars from the retentate. For the investigated GE1812C-34D membrane, this optimum is around 25% w/w.

6. ACKNOWLEDGEMENTS

This work was carried out as part of a project of the Institute for Sustainable Process Technology (ISPT), The Netherlands: project number CM-20-05.

NOMENCLATURE

1	a	Chemical activity [dimensionless]
2	C	Concentration [mol/m^3]
3	C_T	Total molar concentration [mol/m^3]
4	D	Mutual Diffusion coefficient [m^2/s]
5	D_p	Diffusion coefficient inside the pore[m^2/s]
6	d	Diameter of the water molecule [m]
7	d_h	Hydraulic diameter [m]
8	f_R	Frequency [dimensionless]
9	h_f	Hydration number for fructose [dimensionless]
10	J	Volumetric flux [m/s]
11	K_c	Hindrance coefficient for convection [dimensionless]
12	K_d	Hindrance coefficient for diffusion [dimensionless]
13	k	Mass transfer coefficient [m/s]
14	Mw	Molecular weight [g/mol]
15	m	Number of components (including water as component m) [dimensionless]
16	N	Molar flux [mol/(m^{2}s)]
17	n_H	Hydration number [dimensionless]
18	P	Transmembrane Pressure [Pa]
19	P_e	Effective Pressure [Pa]
20	P_n	Total number of pores per area of membrane [m^{-2}]
21	Pe	Péclet number [dimensionless]
22	R	Gas constant [J/(K mol)]
23	Re	Reynolds number [dimensionless]
24	r_G	Average radius according to the Simplified Capsular approach [m]
25	r_i	Radius of molecule i [m]
26	r_p	Radius of the pore [m]
27	r_S	Stokes' radius [m]

1	r^*	Mean radius [m]
2	Sc	Schmidt number [dimensionless]
3	Sh	Sherwood number [dimensionless]
4	s	Number of segments per solute [dimensionless]
5	T	Temperature [K]
6	u	Linear velocities [m/s]
7	$\bar{v}$	Molar volume [m^3/mol]
8	v	Cross flow velocity [m/s]
9	Y	Variable that contains the contribution of the pressure gradient [dimensionless]
10	x	Molar fraction [dimensionless]
11		
12	**Greek letters**	
13	δ_{ij}	Kronecker delta operator [dimensionless]
14	ΔZ	Membrane thickness [m]
15	Đ	Maxwell-Stefan diffusion coefficient [m^2/s]
16	Γ	Thermodynamic factor [dimensionless]
17	Π	Osmotic Pressure [Pa]
18	γ	Activity coefficient [dimensionless]
19	δ	Concentration polarization layer thickness [m]
20	η	Viscosity [Pa s]
21	λ	Ratio between the molecular and pore radii [dimensionless]
22	μ	Chemical Potential [J/mol]
23	ρ	Density [kg/m^3]
24	σ	standard deviation of the pore size distribution [m]
25	φ	Partition coefficient [dimensionless]
26	$\hat{\phi}_i$	Steric hindrance [dimensionless]
27		

APPENDICES

A. Calculation of the concentration polarization thickness δ.

According to Wesseling and Krisna, depending on the system, the diffusivity of the fastest or the slowest species can be used in the estimation of δ as described in Eqs. A1 –A4 [14]. In this study, the diffusivity of the slowest molecule (DP7) was used to estimate δ.

$$\delta = \frac{d_h}{Sh} \tag{A1}$$

$$Sh = 0.065\, Re^{0.875}\, {Sc_i}^{0.25} \tag{A2}$$

$$Re = \frac{\rho_r\, v\, d_h}{\eta_r} \tag{A3}$$

$$Sc_i = \frac{\eta_r}{\rho_r\, D_i} \tag{A4}$$

The range of validity of Eq. A2 has been tested for 100 < Re > 1000 [41]. Re decreases as the viscosity increases due to high solutes concentration. At the conditions analysed in this study, we obtained Re numbers from 190 to 85. Although partially out of the range, the Sh equation was still considered valid since at very high concentrations (due to the low permeate flux) the concentration profiles become less steep in the film layer, thus high accuracy is not needed. Bandini et al presented promising new Sh equations specifically for 1812 spiral wound modules which are promising in terms of accuracy [42]. In this study, however, we do not use this new Sh equations in order to keep consistency with the model used in our previous study in which we estimated the pore size distribution of the membrane.

To calculate the hydraulic diameter d_h and the cross-flow velocity v in spiral wound membranes, the procedure presented by Schock and Miquel can be used [41]. ρ_r and η_r stand for the density and the viscosity of the retentate. D_i^{∞} can be calculated using the empirical relation proposed by Sano and Yamamoto in 1992 (Eq.A5), which links D_i^{∞} with the molecular weight of the sugar (Mw_i) [43].

$$D_i^{\infty} = \frac{T}{9.5 \cdot 10^{13}\, Mw_i^{1/3}\, \eta_{H2O}} \tag{A5}$$

The viscosity in any part of the system can be calculated based on the composition of the mixture. Chirife et al. presented a simple viscosity relation (Eq. A6) to calculate the viscosity of sugar solutions using the average molar mass of the mixture (Mw_{av}) and a parameter E. Parameter E can be calculated from a linear relation as it was done in a previous study[44] [45].

$$\eta = \eta_{H2O} \exp\left(E \sum_{i=1}^{m-1} x_i\right) \tag{A6}$$

$$E = 0.162\, Mw_{av} - 9.842$$

B. Calculation of activity coefficient (γ) from hydration numbers.

The chemical activity (a) is interpreted as an effective molar fraction. Thus, the activity of solute i in a mixture with other solutes and water results in:

$$a_i = \frac{n_i}{\left(\sum_{j=1}^{m} n_j\right) - n_{hyd}} \tag{B1}$$

where n is the number of moles, the term in brackets represent the sum of moles of all the components in the mixture and n_{hyd} is the number of water moles bound to the solutes. Then, If we divide every term by the total number of moles (the term in brackets), we obtain:

$$a_i = \frac{x_i}{1 - \frac{n_{hyd}}{\left(\sum_{j=1}^{m} n_j\right)}} \tag{B2}$$

The activity coefficients γ are interpreted according to Henry's law. Therefore, the reference state is the solute with only solvent molecules in its surrounding, and the next relations hold:

$$\gamma_i \to 1 \quad as \quad x_i \to 0 \quad (solutes) \tag{B3}$$

$$\gamma_m \to 1 \quad as \quad x_m \to 1 \quad (solvent) \tag{B4}$$

Considering the aforementioned definitions, the activity coefficient for solute i is:

$$\gamma_i = \frac{a_i}{x_i} = \frac{\frac{x_i}{1 - \frac{n_{hyd}}{\left(\sum_{j=1}^{m} n_j\right)}}}{x_i} = \frac{1}{1 - \frac{n_{hyd}}{\left(\sum_{j=1}^{m} n_j\right)}} \tag{B5}$$

n_{hyd} represents the number of moles of water in the hydration layers of all the sugar molecules in the mixture. Assuming that the segments (fructose in the case of fructooligosaccharides) of each type of sugar behave in a similar way we can generalize in the following way:

$$n_{hyd} = h_f n_{seg} \tag{B6}$$

$$n_{seg} = \sum_{i=k}^{m-1} n_k s_k \tag{B7}$$

Where h_f is the hydration number of one segment (in our case fructose) and s is the degree of polymerization of each type of sugar (number of segments). We postulate that h_f is constant for all segments, and is independent of s. Consequently:

$$x_{seg} = \frac{n_{seg}}{n_{total}} = \frac{n_{seg}}{\sum_{j=1}^{m} n_j} \tag{B8}$$

x_{seg} is not precisely a molar fraction because the total number of moles takes into account the complete sugars and not their segments. It is useful to simplify Eq. B5 as follows:

$$\frac{n_{hyd}}{\sum_{j=1}^{m} n_j} = h_f \, x_{seg} \tag{B9}$$

$$\gamma = \frac{1}{1 - h_f \, x_{seg}} \tag{B10}$$

C. Calculation of the membrane retention $x_{i,p(r)}$.

Due to the principle of mass conservation, the flux of solutes inside the pore is similar to the flux of solutes in the permeate just outside the pore, thus: $C_T x_i u_i = C_{Tp} x_{p,i} u_p$. Assuming that $C_T \approx C_{Tp}$, and considering that the velocity of species i in the permeate (just outside the pore) is similar to that of water $\left(u_p = u_m = u\right)$, we can simplify Eq. 15 to obtain:

$$x_{p,i}u = K_{c,i}x_i u - D_{p,i}\frac{dx_i}{dz} - D_{p,i}\frac{x_i\,\bar{v}_i}{RT}\frac{dP}{dz} \quad \text{(C1)}$$

At the right side of the Eq. C1, the first term represent the transport due to convection, in which x_i is the local molar fraction and u is the solution velocity. u can be estimated using the Hagen-Poiseuille relation (Eq. C2). This relation describes convection of a liquid through a cylindrical tube with laminar flow. Here, r represents the pore radius and dP_e is the effective pressure over the pore. A negative sign should be included in this definition considering that ΔP_e is negative in the direction of u.

$$u = \frac{r^2}{8\eta}\left(-\frac{dP_e}{dz}\right) = -\frac{r^2\Delta P_e}{8\eta\Delta z} \quad \text{(C2)}$$

The second term in Eq. C1 is the diffusion term, in which D_p is the diffusion coefficient inside the pore. To estimate it, Eq. C3 can be used, in which the effect of the diffusion hindrance (Kd) and the increment in viscosity due to the confinement of water is considered (Eq. C4). Here d is the thickness of the layer of water with increased viscosity that is estimated to be 0.28 nm.

$$D_{p,i} = K_{d,i}D_i^{\infty}\frac{\eta}{\eta_0} \quad \text{(C3)}$$

$$\frac{\eta}{\eta_0} = 1 + 18\left(\frac{d}{r}\right) - 9\left(\frac{d}{r}\right)^2 \quad \text{(C4)}$$

The third term of Eq. C1 is the pressure effect in the transport. Under diluted conditions, this is the least important transport mechanism for solutes ($i \neq m$) in membrane filtration processes.

The meaning and relevance of the hindrance factors (K_c and K_d) were reviewed by Deen (1987) [46]. The chosen expressions to calculate these hindrance coefficients must be applicable to any λ value from 0 to 1 ($\lambda = r_i/r_{pore}$). This is critical when taking into account pore size distributions in the model. The expression for K_c can be taken from Dechadilok and Deen (2006) [47] and the equation for K_d can be obtained from the work of Bungay and Brenner (1973) [48]. Eqs. C5 and C6 were developed for spherical solutes; in the case of elongated molecules (as in this study), K_c can be considered equal to 1 for molecules bigger than DP3 [49], and K_d can only be roughly estimated using the Stokes radius (r_s) as done in our previous study [13].

$$K_c = \frac{1 + 3.867\lambda - 1.907\lambda^2 - 0.834\lambda^3}{1 + 1.867\lambda - 0.741\lambda^2} \tag{C5}$$

1

$$K_d = \frac{6\pi}{K_t} \tag{C6}$$

$$K_t = \frac{9}{4}\pi^2\sqrt{2}\,(1-\lambda)^{-\frac{5}{2}}\left[1 + \sum_{n=1}^{2} a_n(1-\lambda)^n\right] + \sum_{n=0}^{4} a_{n+3}\,\lambda^n$$

$$a_1 = -\frac{73}{60}, a_2 = \frac{77.293}{50.400}, a_3 = -22.5083, a_4 = -5.6117, a_5 = -0.3363,$$

$$a_6 = -1.216, a_7 = 1.647$$

2 To solve Eq. C1 a procedure similar to the one of Bowen and Welfoot with the Steric Pore Model was
3 followed [2, 32]. Thus, after linearizing $\frac{dP}{dz}$ in Eq. C1, an expression for $\frac{dx_i}{dz}$ can be obtained (Eq. C7).
4 Here a new variable Y_i, which is considered constant along the thickness of the membrane, has been
5 defined. Y represents the contribution of the pressure gradient in the transport of each solute.

$$\frac{dx_i}{dz} = \frac{u}{D_{p,i}}\left[(K_{c,i} - Y_i)x_i - x_{p,i}\right] \tag{C7}$$

$$Y_i = \frac{D_{p,i}\bar{v}_i}{RT\ V}\frac{dP}{dz} = -\frac{8\eta D_{p,i}\bar{v}_i}{RT\ r^2}\frac{\Delta P}{\Delta P_e} \tag{C8}$$

6

7 Under concentrated conditions $\Delta P \neq \Delta P_e$, because ΔP_e is a function of the osmotic pressure (Π),
8 which counteracts the effect of ΔP. x_i can be integrated (from Eq. C7) over the thickness of the
9 membrane using the boundary conditions given in Eq. C9, in which two different partition coefficients
10 are defined. Additionally, a modified version of the Péclet number Pe_i' has been used in the derivation
11 to group some variables (Eq. C10). As a result, an expression for the porewise permeate mole fraction
12 $x_{i,p(r)}$ can be obtained (Eq. C11).

$$x_0 = \varphi_{w,i}\, x_{w,i} \tag{C9}$$

$$x_{end} = \varphi_{p,i}\, x_{p,i}$$

$$Pe_i' = \frac{V}{D_{p,i}}\Delta z \left(K_{c,i} - Y_i\right) = -\frac{r^2 \Delta P_e}{8\eta D_{p,i}} \left(K_{c,i} - Y_i\right) \tag{C10}$$

$$x_{i,p(r)} = \frac{\left(K_{c,i(r)} - Y_{i(r)}\right)\varphi_{w,i}\, x_{w,i}\, exp\left(Pe'_{i(r)}\right)}{\left(K_{c,i(r)} - Y_{i(r)}\right)\varphi_{p,i(r)} - 1 + exp\left(Pe'_{i(r)}\right)} \tag{C11}$$

D. Calculation of water activity (*aw*) from composition.

As done previously with the activity of i, water activity can also be represented as an effective molar fraction. For a system of m-1 solutes (j) and water, we obtain:

$$a_{H2O} = \frac{n_{H2O} - n_{hyd}}{\sum_{j=1}^{m} n_j - n_{hyd}} \tag{D1}$$

If we divide the numerator and denominator of Eq. D1 by the total number of moles ($\sum_{j=1}^{m} n_j$), we obtain:

$$a_{H2O} = \frac{\frac{n_{H2O}}{\sum_{j=1}^{m} n_j} - \frac{n_{hyd}}{\sum_{j=1}^{m} n_j}}{1 - \frac{n_{hyd}}{\sum_{j=1}^{m} n_j}} \tag{D2}$$

Considering the definition in Eq. B9, we can simplify the expression above to:

$$a_{H2O} = \frac{x_{H2O} - h_f x_{seg}}{1 - h_f x_{seg}} \tag{D3}$$

Since a_i and a_{H2O} are effective mole fractions, they should sum 1 all together:

$$\sum_{i=1}^{m-1} \frac{x_i}{1-h_f\,x_{seg}} + \frac{x_{H2O}-h_f x_{seg}}{1-h_f x_{seg}} = \frac{\sum_{i=1}^{m-1} x_i + x_{H2O} - h_f x_{seg}}{1-h_f x_{seg}} = \frac{1-h_f x_{seg}}{1-h_f x_{seg}} = 1 \quad \text{(D4)}$$

REFERENCES

[1] R. Baker, Membrane Technology and Applications 2nd ed., Wiley, California, USA, 2004.

[2] W.R. Bowen, J.S. Welfoot, Modelling the performance of membrane nanofiltration—critical assessment and model development, Chem. Eng. Sci., 57 (2002) 1121-1137.

[3] O. Kedem, A. Katchalsky, Thermodynamic analysis of the permeability of biological membranes to non-electrolytes, Biochim. Biophys. Acta, 27 (1958) 229-246.

[4] M.A.J.S. van Boekel, Kinetic Modeling of Reactions In Foods, CRC Press, 2008.

[5] J. Straatsma, G. Bargeman, H.C. van der Horst, J.A. Wesselingh, Can nanofiltration be fully predicted by a model?, J. Membr. Sci., 198 (2002) 273-284.

[6] G. Bargeman, J.M. Vollenbroek, J. Straatsma, C.G.P.H. Schroën, R.M. Boom, Nanofiltration of multi-component feeds. Interactions between neutral and charged components and their effect on retention, J. Membr. Sci., 247 (2005) 11-20.

[7] R.C. Kuhn, F. Maugeri Filho, V. Silva, L. Palacio, A. Hernández, P. Prádanos, Mass transfer and transport during purification of fructooligosaccharides by nanofiltration, J. Membr. Sci., 365 (2010) 356-365.

[8] W. Li, J. Li, T. Chen, Z. Zhao, C. Chen, Study on nanofiltration for purifying fructo-oligosaccharides: II. Extended pore model, J. Membr. Sci., 258 (2005) 8-15.

[9] C.W. van Oers, M.A.G. Vorstman, R.v.d. Hout, P.J.A.M. Kerkhof, The influence of thermodynamic activity on the solute rejection in multicomponent systems, J. Membr. Sci., 136 (1997) 71-87.

[10] J. Luo, Y. Wan, Effect of highly concentrated salt on retention of organic solutes by nanofiltration polymeric membranes, J. Membr. Sci., 372 (2011) 145-153.

[11] R. A. Robinson, R. H. Stokes, Activity coefficients in aqueous solutions of sucrose, mannitol and their mixtures at 25°, 1961.

[12] A.A. Hussain, S.K. Nataraj, M.E.E. Abashar, I.S. Al-Mutaz, T.M. Aminabhavi, Prediction of physical properties of nanofiltration membranes using experiment and theoretical models, J. Membr. Sci., 310 (2008) 321-336.

[13] V. Aguirre Montesdeoca, J. Bakker, R.M. Boom, A.E.M. Janssen, A. Van der Padt, Ultrafiltration of non-spherical molecules, J. Membr. Sci., 570-571 (2019) 322-332.

[14] J.A. Wesselingh, R. Krishna, Mass Transfer in Multicomponent Mixtures, VSSD, Delft, 2000.

[15] S. Postel, S. Wessel, T. Keil, P. Eiselt, M. Wessling, Multicomponent mass transport in organic solvent nanofiltration with solvent mixtures, J. Membr. Sci., 466 (2014) 361-369.
[16] R. Taylor, R. Krishna, Multicomponent Mass Transfer, John Wiley & Sons, Inc, New York, 1993.
[17] H.A. Kooijman, R. Taylor, Estimation of diffusion coefficients in multicomponent liquid systems, Industrial & Engineering Chemistry Research, 30 (1991) 1217-1222.
[18] X. Liu, T.J.H. Vlugt, A. Bardow, Maxwell–Stefan diffusivities in liquid mixtures: Using molecular dynamics for testing model predictions, Fluid Phase Equilib., 301 (2011) 110-117.
[19] G. Scatchard, THE HYDRATION OF SUCROSE IN WATER SOLUTION AS CALCULATED FROM VAPOR-PRESSURE MEASUREMENTS, J. Am. Chem. Soc., 43 (1921) 2406-2418.
[20] M.J. Blandamer, J.B.F.N. Engberts, P.T. Gleeson, J.C.R. Reis, Activity of water in aqueous systems; A frequently neglected property, Chem. Soc. Rev., 34 (2005) 440-458.
[21] P. Walstra, Physical Chemistry of Foods, Marcel Dekker Inc., New York, 2003.
[22] A. Gharsallaoui, B. Rogé, J. Génotelle, M. Mathlouthi, Relationships between hydration number, water activity and density of aqueous sugar solutions, Food Chem., 106 (2008) 1443-1453.
[23] A. Burakowski, J. Gliński, Hydration Numbers of Nonelectrolytes from Acoustic Methods, Chem. Rev., 112 (2012) 2059-2081.
[24] E.D. Glandt, Distribution equilibrium between a bulk phase and small pores, AlChE J., 27 (1981) 51-59.
[25] E.M. Renkin, Filtration, diffusion, and molecular sieving through porous cellulose membranes, The Journal of general physiology, 38 (1954) 225-243.
[26] J.C. Giddings, E. Kucera, C.P. Russell, M.N. Myers, Statistical theory for the equilibrium distribution of rigid molecules in inert porous networks. Exclusion chromatography, The Journal of Physical Chemistry, 72 (1968) 4397-4408.
[27] T.R. Noordman, T.H. Ketelaar, F. Donkers, J.A. Wesselingh, Concentration and desalination of protein solutions by ultrafiltration, Chem. Eng. Sci., 57 (2002) 693-703.
[28] G. Bargeman, J.B. Westerink, C.F.H. Manuhutu, A.t. Kate, The effect of membrane characteristics on nanofiltration membrane performance during processing of practically saturated salt solutions, J. Membr. Sci., 485 (2015) 112-122.
[29] B.D. Mitchell, W.M. Deen, Effect of concentration on the rejection coefficients of rigid macromolecules in track-etch membranes, J. Colloid Interface Sci., 113 (1986) 132-142.
[30] Y.-X. Yu, J. Wu, Structures of hard-sphere fluids from a modified fundamental-measure theory, The Journal of Chemical Physics, 117 (2002) 10156-10164.
[31] Y.-X. Yu, J. Wu, Y.-X. Xin, G.-H. Gao, Structures and correlation functions of multicomponent and polydisperse hard-sphere mixtures from a density functional theory, The Journal of Chemical Physics, 121 (2004) 1535-1541.

[32] W.R. Bowen, J.S. Welfoot, Modelling of membrane nanofiltration—pore size distribution effects, Chem. Eng. Sci., 57 (2002) 1393-1407.
[33] S. Bandini, V. Morelli, Effect of temperature, pH and composition on nanofiltration of mono/disaccharides: Experiments and modeling assessment, J. Membr. Sci., 533 (2017) 57-74.
[34] J.M. Campbell, L.L. Bauer, G.C. Fahey, A.J.C.L. Hogarth, B.W. Wolf, D.E. Hunter, Selected Fructooligosaccharide (1-Kestose, Nystose, and 1F-β-Fructofuranosylnystose) Composition of Foods and Feeds, J. Agric. Food. Chem., 45 (1997) 3076-3082.
[35] A.K.H. D'Haese, I. De Leersnyder, P. Vermeir, A.R.D. Verliefde, On negative rejection of uncharged organic solutes in forward osmosis, J. Membr. Sci., 548 (2018) 22-31.
[36] A.E. Yaroshchuk, Negative rejection of ions in pressure-driven membrane processes, Adv. Colloid Interface Sci., 139 (2008) 150-173.
[37] L.S. Darken, Diffusion of carbon in austenite with a discontinuity in composition, Trans. AIME., 180 (1949) 430-438.
[38] R. Krishna, Uphill diffusion in multicomponent mixtures, Chem. Soc. Rev., 44 (2015) 2812-2836.
[39] R. Krishna, Diffusing uphill with James Clerk Maxwell and Josef Stefan, Current Opinion in Chemical Engineering, 12 (2016) 106-119.
[40] W.R. Bowen, A.W. Mohammad, N. Hilal, Characterisation of nanofiltration membranes for predictive purposes — use of salts, uncharged solutes and atomic force microscopy, J. Membr. Sci., 126 (1997) 91-105.
[41] G. Schock, A. Miquel, Mass transfer and pressure loss in spiral wound modules, Desalination, 64 (1987) 339-352.
[42] S. Bandini, V. Morelli, Mass transfer in 1812 spiral wound modules: Experimental study in dextrose-water nanofiltration, Sep. Purif. Technol., 199 (2018) 84-96.
[43] Y. Sano, S. Yamamoto, Mutual Diffusion Coefficient of Aqueous Sugar Solutions, J. Chem. Eng. Jpn., 26 (1993) 633-636.
[44] J. Chirife, M.P. Buera, A simple model for predicting the viscosity of sugar and oligosaccharide solutions, J. Food Eng., 33 (1997) 221-226.
[45] V. Aguirre Montesdeoca, A. Van der Padt, R.M. Boom, A.E.M. Janssen, Modelling of membrane cascades for the purification of oligosaccharides, J. Membr. Sci., 520 (2016) 712-722.
[46] W. Deen, Hindered transport of large molecules in liquid-filled pores, AlChE J., 33 (1987) 1409-1425.
[47] P. Dechadilok, W.M. Deen, Hindrance Factors for Diffusion and Convection in Pores, Industrial & Engineering Chemistry Research, 45 (2006) 6953-6959.
[48] P.M. Bungay, H. Brenner, The motion of a closely-fitting sphere in a fluid-filled tube, Int. J. Multiphase Flow, 1 (1973) 25-56.

[49] B. Agasanapura, R.E. Baltus, C. Tanneru, S. Chellam, Membrane rejection of nonspherical particles: Modeling and experiment, AlChE J., 59 (2013) 3863-3873.